SECURITY INFORMATION [redacted]

CLASSIFICATION CANCELLED

~~CONFIDENTIAL~~

Copy 1
RM SL53D28

REC'D APR 29 1953

NACA

CLASSIFICATION CANCELLED

RESEARCH MEMORANDUM

for the

Bureau of Aeronautics, Department of the Navy

A TRANSONIC WIND-TUNNEL INVESTIGATION OF THE TRIM AND DYNAMIC RESPONSE CHARACTERISTICS OF THE HORIZONTAL TAIL OF A 1/7-SCALE MODEL OF THE COMPLETE TAIL OF THE GRUMMAN XF10F-1 AIRPLANE

By Arvo A. Luoma

Langley Aeronautical Laboratory
Langley Field, Va.

CLASSIFICATION CANCELLED

Authority NACA RESEARCH ABSTRACTS
and Reclassification Notice No. 99

Date 4/6/56 By OCS

[redacted]

NATIONAL ADVISORY COMMITTEE
FOR AERONAUTICS

WASHINGTON

APR 28 1953

FILE COPY
To be returned to
the files of the National
Advisory Committee
for Aeronautics
Washington, D.C.

16

CLASSIFICATION CANCELLED

~~CONFIDENTIAL~~

CONFIDENTIAL
CLASSIFICATION CANCELLED

NATIONAL ADVISORY COMMITTEE FOR AERONAUTICS

RESEARCH MEMORANDUM

for the

Bureau of Aeronautics, Department of the Navy

A TRANSONIC WIND-TUNNEL INVESTIGATION OF THE TRIM AND DYNAMIC RESPONSE CHARACTERISTICS OF THE HORIZONTAL TAIL OF A 1/7-SCALE MODEL OF THE COMPLETE TAIL OF THE GRUMMAN XF10F-1 AIRPLANE

By Arvo A. Luoma

SUMMARY

An investigation was made of the trim and dynamic response characteristics of the free-floating horizontal tail of a 1/7-scale model of the complete tail of the Grumman XF10F-1 airplane in the Langley 8-foot transonic tunnel at Mach numbers up to 1.13. The complete tail was mounted in the tunnel on a 3° conical support body. Various configurations were investigated.

A loss in damping of the horizontal tail at transonic speeds was shown by both tunnel and flight tests. The loss in damping extended over a greater Mach number range and the maximum loss occurred at a higher Mach number in the tunnel tests. Large-amplitude oscillations of the horizontal tail of the basic configuration which occurred at low supersonic Mach numbers appeared to be primarily due to the vertical tail of the basic configuration and the interference effects associated with this tail. Secondary factors contributing to the development of the large-amplitude oscillations of the horizontal tail of the basic configuration were probably the loss in damping of the horizontal tail at transonic speeds and the turbulence of the airstream itself.

INTRODUCTION

Flight tests have been made by the NACA of a wingless rocket-powered vehicle equipped with a 1/7-scale model of the complete tail of the

CONFIDENTIAL
CLASSIFICATION CANCELLED

Grumman XF10F-1 airplane (ref. 1). This tail included a free-floating horizontal tail controlled by a canard servoplane which, on the actual airplane, is in turn controlled by the pilot. The flight tests revealed trim changes of the free-floating horizontal tail at transonic speeds which were considered to be undesirable, and undamped oscillations of the horizontal tail in a localized Mach number range at a Mach number of approximately 0.98. At the request of the Bureau of Aeronautics, Department of the Navy, a brief investigation was made in the Langley 8-foot transonic tunnel of a 1/7-scale model of the complete tail of the Grumman XF10F-1 airplane for the purpose of studying the characteristics of this tail at transonic speeds in a somewhat more detailed manner than was practicable in the flight tests.

The wind-tunnel tests provided information on the trim angle of the horizontal tail for two deflections of the canard servoplane, on the pressures over the vertical tail and the support body on which the tail was mounted, on the dynamic response of the horizontal tail to an abrupt displacement of the canard servoplane, and on shock formations at the nose of the canard servoplane and the trailing edge of the main lifting surface of the horizontal tail. An indication of the interference effects associated with the vertical tail was obtained from additional tests with the horizontal tail supported on an auxiliary small-chord sweptforward vertical tail.

SYMBOLS

The term "horizontal tail" as used herein refers to the combination of the main lifting surface (which includes a stabilizer and a "stabilator") of the horizontal tail, the boom, and the canard servoplane. See figure 1 for identification of parts of model and positive directions of angles. The symbols used in this paper are defined as follows:

b exponential damping coefficient in e^{-bt}

C_m pitching-moment coefficient of horizontal tail, $\frac{M'}{qS\bar{c}}$

$C_{m_{i_h}}$ rate of change of pitching-moment coefficient of horizontal tail with incidence of horizontal tail, $\frac{\partial C_m}{\partial i_h}$

$C_{m_{\dot{i}_h}}$ rate of change of pitching-moment coefficient of horizontal tail with parameter $\frac{\dot{i}_h\bar{c}}{2V}$, $\frac{\partial C_m}{\frac{\partial \dot{i}_h\bar{c}}{2V}}$

$\bar{c}$	mean aerodynamic chord of main lifting surface of horizontal tail
e	base of natural system of logarithms
I	moment of inertia of horizontal tail about pivot axis of horizontal tail
i_h	incidence of horizontal tail, measured by angle between plane of main lifting surface (stabilizer) of horizontal tail and center line of 3° conical support body
$\dot{i}_h$	rate of change of incidence of horizontal tail with time, $\frac{di_h}{dt}$
Δi_h	change in incidence of horizontal tail from trim position, $i_h - (i_h)_{trim}$
$(i_h)_{trim}$	trim (floating) angle of horizontal tail, corresponding to zero moment of forces on horizontal tail about pivot axis of horizontal tail
M	Mach number of undisturbed stream
M'	pitching moment of horizontal tail about pivot axis of horizontal tail
M_l	local Mach number of stream over a point on model
P	period
q	dynamic pressure of undisturbed stream
R	Reynolds number based on $\bar{c}$
S	area of main lifting surface of horizontal tail
$T_{1/2}$	time to damp to one-half amplitude, $\frac{\log_e 1/2}{b}$
t	time
V	velocity of undisturbed stream

α_b angle of attack of 3° conical support body, measured by angle between center line of 3° conical support body and direction of undisturbed stream (no model in tunnel)

α_h angle of attack of horizontal tail, measured by angle between plane of main lifting surface (stabilizer) of horizontal tail and mean direction of flow (determined from surveys with 3° conical support body alone in tunnel) in region occupied by horizontal tail

δ_c deflection of canard servoplane, measured by angle between plane of canard servoplane and plane of main lifting surface (stabilizer) of horizontal tail

δ_e deflection of stabilator, measured by angle between plane of stabilator and plane of stabilizer

θ_b inclination of 3° conical support body, measured by angle between horizontal plane and center line of 3° conical support body

θ_h inclination of horizontal tail, measured by angle between horizontal plane and plane of main lifting surface (stabilizer) of horizontal tail

θ_{w_b} inclination (in vertical plane) of flow approaching 3° conical support body, measured by angle between horizontal plane and direction of undisturbed stream (no model in tunnel)

θ_{w_h} local inclination (in vertical plane) of flow approaching horizontal tail, measured by angle between horizontal plane and local direction of flow (determined from surveys with 3° conical support body alone in tunnel) in region occupied by horizontal tail

$\bar{\theta}_{w_h}$ mean inclination (in vertical plane) of flow approaching horizontal tail, measured by angle between horizontal plane and mean direction of flow (determined from surveys with 3° conical support body alone in tunnel) in region occupied by horizontal tail

APPARATUS AND METHODS

Tunnel

The tests were made in the Langley 8-foot transonic tunnel. This tunnel operates at a stagnation pressure approximately equal to atmospheric pressure. The tunnel throat is of dodecagonal cross section with axial slots located at the vertices of the twelve wall panels. The slotted design permits model testing at speeds through sonic velocity (refs. 2 and 3). Information on the design of the slotted test section of the Langley 8-foot transonic tunnel is given in reference 4 and on the calibration of the flow in this tunnel in reference 3.

Models and Instrumentation

The 1/7-scale model of the complete tail of the Grumman XF10F-1 airplane was mounted in the wind tunnel on a 3° conical support body. The 3° cone was chosen as the supporting body in order to minimize the shock-reflection interference effects of a supporting body at low supersonic Mach numbers on the flow over the tail. Photographs and dimensions of the model are given in figures 2 and 3, respectively, and the specifications of the tail are given in table I. The location of the model in the wind tunnel is shown in figure 4. Three guy wires were used to improve the rigidity of the model support system and these wires are indicated in figure 4.

The horizontal tail was free to pivot, within limits, about an axis perpendicular to the plane of the vertical tail as indicated in figure 3. Prior to the tests, the horizontal tail was statically balanced about the pivot axis. The mass and moment of inertia (about the pivot axis) of the horizontal tail for the various configurations are given in the following table:

Configuration	Mass, slugs	Moment of inertia, slug-ft^2
Basic (fig. 3).	0.340	0.156
Basic less canard servoplane.	.342	.140
Basic plus small image fin (fig. 5) . . .	.348	.153
Basic plus large image fin (fig. 5) . . .	.353	.155
Combination with sweptforward vertical tail (fig. 6)	.341	.155
Combination with sweptforward vertical tail less canard servoplane	.343	.139

The canard servoplane was hinged as indicated in figure 3, and was capable of being pneumatically pulsed between deflection limits which could be adjusted to desired values. For the present tests, the canard servoplane was pulsed in a square-wave motion with a frequency of 0.49 cycle per second.

The stabilator was linked to the vertical tail in a way such that an angular displacement of the horizontal tail relative to the vertical tail resulted in a deflection of the stabilator relative to the stabilizer, the direction of deflection of the stabilator being the same as that of the horizontal tail. The linkage used in the present tests gave a rate of change of stabilator deflection with incidence of the horizontal tail $d\delta_e/di_h$ of 1, and a value of stabilator deflection of 0° when the incidence of the horizontal tail was 0°. The hinge line of the stabilator is indicated in figure 3.

Two image fins designated herein as "small" and "large" were attached in turn to the boom as shown in figure 5, and tests were made of these configurations. The airfoil section of the fins was an NACA 64A008. The fins were tested in an attempt to improve the trim variation of the horizontal tail with Mach number by providing a counterinterference effect to that associated with the vertical tail. An auxiliary small-chord sweptforward vertical tail was used to replace the basic vertical tail for some of the tests, and these tests in combination with those of the basic configuration gave some indication of the interference effects of the vertical tail. Dimensions of the auxiliary vertical tail are given in figure 6. A photograph of the horizontal tail in combination with the auxiliary vertical tail in the Langley 8-foot transonic tunnel is shown as figure 7. The nose of the canard servoplane was located in the tunnel at the 70-inch station for the tests with the auxiliary vertical tail, the same location as that for the basic configuration.

A time record of the incidence of the horizontal tail i_h was obtained with a slide-wire indicator coupled to a Heiland recording galvanometer. The inclination of the horizontal tail θ_h for steady, trim conditions was measured with a cathetometer. A time record of the change in inclination of the 3° conical support body θ_b due to flexibility of the support system was obtained on a film recorder in combination with an optical angle-measuring system utilizing a small mirror on the upper surface of the 3° conical support body. A survey cone was used in determining the angularity of the flow in the region of the horizontal tail (3° conical support body alone in tunnel) and the angularity of the flow approaching the 3° conical support body (no model in tunnel). The survey cone had an included angle of 10° and was attached to a 1-inch-diameter cylindrical tube. Two static-pressure orifices (0.015-inch diameter) were located $2\frac{3}{4}$ inches from the vertex of the cone and 180° apart.

A few static-pressure orifices were installed on the model. These orifices included a row on one surface of the basic vertical tail adjacent to the horizontal tail and a row on the 3° conical support body. The locations of the orifices are shown in figure 3.

Test Procedure

Aerodynamic data were obtained at Mach numbers of 0.70, 0.85, 0.925, 0.975, 1.00, 1.02, 1.035, 1.05, 1.10, and at a maximum Mach number of approximately 1.13. For some of the runs, intermediate values of Mach number were also included. At a given Mach number, the canard servoplane was pulsed between its deflection limits and a time record of the incidence of the oscillating horizontal tail was taken; conjointly, a time record of the vibration of the 3° conical support body was made. The duration of the pulsed records was approximately 6 seconds. The trim position of the horizontal tail with the canard servoplane locked in each of its limit positions was determined with a cathetometer and also by means of a record (approximately 2-seconds duration) obtained on the slide-wire recorder. At the trim conditions, pressure-distribution data on the basic vertical tail and the 3° conical support body were photographically obtained, and schlieren data were taken when shock phenomena were evident.

The mean angle of attack of the 3° conical support body α_b was 0° for these tests. The change in angle of attack of the 3° conical support body $\Delta\alpha_b$ as a result of vibration of the 3° conical support body was less than ±0.05° from the mean value for most Mach numbers; at low supersonic Mach numbers where undamped oscillations of the horizontal tail occurred, the change $\Delta\alpha_b$ amounted to ±0.2°.

The configurations tested included the basic configuration (fig. 3), the basic configuration less the canard servoplane, the basic configuration plus the small image fin (fig. 5), the basic configuration plus the large image fin (fig. 5), the horizontal tail in combination with the auxiliary small-chord sweptforward vertical tail (fig. 6), and the horizontal tail less the canard servoplane in combination with the small-chord sweptforward vertical tail.

The local inclination of the flow approaching the horizontal tail θ_{w_h} (obtained with the 3° conical support body alone in the tunnel) was determined with the 10° survey cone at distances of 9.5 inches, 13.9 inches, and 17.5 inches from the center line of the 3° conical support body. The inclination of the center line of the survey probe was approximately 0°, and the probe was positioned longitudinally in the tunnel so that the static-pressure orifices of the probe were located at the same longitudinal tunnel station at which the pivot axis of

the horizontal tail was located. The survey cone was calibrated with no model in the tunnel at inclinations from -2° to 1°, in both the "upright" position and the "inverted" (survey cone rotated 180° about its axis) position.

The Reynolds number of the investigation based on the mean aerodynamic chord of the main lifting surface of the horizontal tail is shown plotted against test Mach number in figure 8.

ACCURACY AND CORRECTIONS

The interference effects of a tunnel boundary at subsonic Mach numbers have been made negligible by means of a slotted test section (see, for example, refs. 2, 3, and 5). At low supersonic Mach numbers, however, reflections from the tunnel boundary of compression and expansion disturbances originating at the model may impinge on the model and modify the aerodynamic characteristics of the model. In the tests of reference 3, it was found that at supersonic Mach numbers less than approximately 1.03, the effect of the reflected compression wave on the model pressure distributions was negligible but that the effect of the reflected expansion waves was noticeable. The over-all effects on forces and moments at Mach numbers less than 1.03, however, can still be small for a particular configuration (refs. 3 and 5). At Mach numbers above 1.04, appreciable effects of both reflected compression and expansion waves on model pressure distributions were observed in the tests of reference 3. Even at these speeds, the over-all effects on forces and moments may be relatively small for a particular configuration (ref. 5). At sufficiently high Mach numbers, the reflected compression wave moves downstream of the model so that the data may be considered to be free of interference. In the present tests, it appeared from the schlieren photographs that the data for the basic configuration were not quite free of interference at the highest Mach number of 1.13 and that the data for the configuration with the sweptforward vertical tail were already free of interference at a somewhat lower Mach number.

The pitching-moment characteristics of the configurations of the present tests are believed to be more sensitive to boundary-reflected disturbances which impinge on the model than those of the configurations of references 3 and 5, since in the present tests, the main lifting surface of the horizontal tail extended to the rear of the boom. Location of the horizontal tail off the center line of the tunnel (fig. 4), however, probably alleviated the reflection effects somewhat in view of the findings of reference 3. The magnitudes of the interference effects for configurations comparable to those tested herein are not known at present. It is suggested, therefore, that the data of the present investigation at supersonic speeds where reflection problems were significant (particularly

at Mach numbers above 1.04, and also at Mach numbers somewhat lower than 1.04 as indicated by the tests of refs. 3 and 5) should be considered to be of uncertain validity. The loss in damping of the horizontal tail at Mach numbers slightly greater than 1, however, is believed to be primarily associated with the characteristics of the model itself.

In the calculation of the local Mach number on the surface of the vertical tail and the 3° conical support body, the total pressure of the free stream was used instead of that of the local flow. The error in Mach number thus introduced was negligible, amounting to less than 0.002 for a normal shock at a Mach number of 1.13.

In the determination of trim angles with a cathetometer, three separate readings were made at each test condition. The scatter of the test points gives some indication of the accuracy of these measurements.

RESULTS AND DISCUSSION

Flow Angularity

The inclination of the flow θ_{w_b} (no model in the tunnel) in the vertical plane in the region of the center line of the Langley 8-foot transonic tunnel was -0.1° (upflow) as shown in figure 9. Data are shown from the investigation reported herein and from that of reference 3, in which a null-pressure-type instrument (3° cone) was used for measuring the angularity of the flow. In the present tests, the inclination of the 3° conical support body θ_b was set at -0.1° to make the angle of attack of the 3° conical support body α_b equal to 0°. The mean inclination of the flow in the region occupied by the horizontal tail $\bar{\theta}_{w_h}$ (obtained with the 3° conical support body alone in the tunnel) was approximately -0.5° (upflow) throughout the Mach number range (fig. 10). This upflow in the present tests corresponded to an angle of attack of the horizontal tail α_h of approximately 0.4° when the incidence of the horizontal tail i_h was 0°.

Model Oscillations

Tracings of representative records of the oscillations of the horizontal tail about the pivot axis are shown in figure 11 for the basic configuration with the canard servoplane both pulsed and locked. At supersonic Mach numbers somewhat greater than 1, the horizontal tail of the basic configuration generally oscillated with large magnitude in a periodic motion, with the canard servoplane either pulsed or locked; the type of record obtained for these conditions is shown in figure 11(c).

At Mach numbers outside the range in which the large-amplitude oscillations occurred, the horizontal tail with the canard servoplane locked oscillated about a mean trim position with a motion which is typified by the record of figure 11(b), and with the canard servoplane pulsed oscillated with motion typified by the record of figure 11(a). The motion of the canard servoplane is also indicated in figure 11(a), although actually no time records were made of this deflection. The motion of the horizontal tail represented by the pulsed record of figure 11(a) appeared to be essentially a damped motion superimposed on the motion represented by the record of figure 11(b). For some of the pulsed records, the damped motion appears to have been modified to an extent which made interpretation of the damping characteristics difficult.

The amplitude of oscillation (from the mean trim position) of the horizontal tail of the basic configuration with the canard servoplane locked is shown in figure 12. These data were obtained from records of the type shown in figures 11(b) and 11(c), which were of approximately 2-seconds duration at each test condition, and are the averaged results from three separate runs. The "maximum amplitude" was the largest recorded displacement from the mean position and the "average amplitude" was the arithmetical average of the individual peak displacements. The amplitude of the oscillation is seen to be appreciable, particularly at low supersonic Mach numbers (fig. 12). The horizontal tail mounted on the sweptforward vertical tail did not exhibit the large-amplitude oscillations at low supersonic Mach numbers (data not presented herein) characteristic of the basic configuration. The frequencies of the horizontal tail of the basic configuration estimated by eye from the oscillation records ranged from approximately 10 cps to 130 cps.

Preliminary measurements of static-pressure fluctuations at several locations along the circuit of the Langley 8-foot transonic tunnel were made during the tests of references 2 and 3. The measurements near the center line of the test section were made with an electrical pressure pickup connected to two static-pressure orifices located 180° apart on the surface of a cone which had an included angle of 3°. A few of those results have been published in reference 3. The pressure fluctuations expressed in terms of flow-angularity changes indicated that the air flow near the center line of the test section at Mach numbers above 0.7 fluctuated in the vertical plane with a maximum amplitude of approximately $\pm 0.5^{\circ}$ and an average amplitude of approximately $\pm 0.2^{\circ}$ in two general frequency bands of approximately 2 to 130 cps and 180 to 400 cps. The amplitude of the oscillations of the horizontal tail of the basic configuration with the canard servoplane locked (fig. 12) corresponded quite closely to the amplitude of the angularity fluctuations of the air flow near the center line of the test section at all Mach numbers except those at low supersonic Mach numbers, where the oscillations of the horizontal tail increased considerably in amplitude. These results together with those of references 6 and 7, which are low-speed investigations on the

effects of turbulence, both in wind tunnels and in the atmosphere, on the oscillatory characteristics of an airplane free to yaw, show that the turbulence of the air flow can be of considerable importance on dynamic response tests.

Figure 13 presents information on the frequency and the maximum amplitude (from the mean position) of the 3° conical support body in combination with the complete tail and the sting support setup. It is seen that the maximum amplitude was only approximately $\pm 0.05^{\circ}$ with a frequency of approximately 9.5 cps for all Mach numbers except those where there was a large loss in the aerodynamic damping of the horizontal tail. At such Mach numbers, the maximum amplitude increased to approximately $\pm 0.2^{\circ}$ and the frequency to approximately 15 cps; this frequency corresponded closely to that of the undamped horizontal tail at these Mach numbers. The fundamental frequency of the combination of the 3° conical support body, the tail model, and the sting support system as determined from tests where the cone was abruptly released after deflection and then permitted to vibrate freely was approximately 9.5 cps.

Damping Characteristics

The period and the time to damp to one-half amplitude of the oscillation of the horizontal tail following a control pulse are shown in figures 14 and 15, respectively. In the determination of the damping constant b (used in getting the time to damp to one-half amplitude) a damping envelope was first faired about the oscillation record and then the amplitude was measured at the beginning and end of a time interval corresponding, generally, to three or four cycles of the oscillation. The results shown in figures 14 and 15 are averaged values from three separate runs. There was considerable variation among the individual values of the time to damp to one-half amplitude used in getting the average value, and it is probable that much of this variation stemmed from the interfering effects of the turbulence of the air flow itself.

Flight and wind-tunnel data on the static pitching-moment derivative $C_{m_{i_h}}$ of the horizontal tail of the basic configuration and on the damping derivative $C_{m_{\dot{i}_h}}$ of the horizontal tail of the basic configuration are shown in figures 16 and 17, respectively. These derivatives were computed from the following equations:

$$C_{m_{i_h}} = -\frac{4\pi^2 I}{57.3 q S \bar{c} P^2}, \text{ per deg}$$

$$C_{m_{\dot{i}_h}} = -\frac{4IV\left(\log_e \frac{1}{2}\right)}{57.3\bar{c}^2 qST_{1/2}}, \text{ per deg}$$

In the computation of the static pitching-moment derivative $C_{m_{i_h}}$, the contribution of the damping term $T_{1/2}$ was negligible, and this term was not included in the equation. The wind-tunnel derivatives were based on the averaged data on period and time to damp to one-half amplitude shown in figures 14 and 15.

The tail configurations tested in the flight investigation (ref. 1) and the wind-tunnel investigation were geometrically the same except for a small difference in the shape of the leading edge of the vertical tail adjacent to and within the horizontal tail. In the wind-tunnel tests, the sweepback of the leading edge of the vertical tail within the horizontal tail was smoothly varied to 90°. In the flight tests, the sweepback of the leading edge of the vertical tail adjacent to and within the horizontal tail was abruptly changed to approximately 0°. The "tunnel" in the horizontal tail was shaped to conform to the vertical tail, and was therefore also somewhat different in the flight and wind-tunnel investigations. The support body for the tail in the wind-tunnel tests was a 3° cone, whereas in the flight tests, the support body was one whose shape was essentially cylindrical.

The flight and wind-tunnel results both showed a general increase in the magnitude of the static pitching-moment derivative $C_{m_{i_h}}$ with Mach number, but the increase was appreciably greater in the tunnel tests (fig. 16). The magnitude of the damping derivative $C_{m_{\dot{i}_h}}$ was smaller in the tunnel tests; the general shapes of the curves against Mach number, however, were the same (fig. 17). The Mach number at which the greatest loss in damping occurred was approximately 0.04 higher in the tunnel tests, and the extent of the loss in damping covered a greater Mach number range in the tunnel tests.

The reasons for the discrepancies between the wind-tunnel and flight static stability and damping results (figs. 16 and 17) have not been established. It may be assumed that at least part of the lack of agreement is associated with differences in the two test techniques, differences in turbulence of the air flow, differences in Reynolds number, differences in model support, and perhaps differences in mechanical friction. Preliminary unpublished flight results appear to indicate that the small difference in the shape of the vertical tail in the flight and wind-tunnel configurations may have affected the Mach number at which the maximum loss in damping occurred.

The turbulence was probably greater in the tunnel tests, and in that case relatively greater amounts of energy from the airstream were probably fed into the oscillatory motion of the horizontal tail during damping in the tunnel tests, as might be inferred from the results of references 6 and 7. The damping derivative obtained in the tunnel tests was an effective value based on three or four cycles of the oscillation. The effect of the number of cycles selected on the magnitude of the damping derivative could not be reliably established from the data of the present tests. It may be presumed, however, that a damping derivative based on the beginning of a damped motion in turbulent flow would tend to be closer in magnitude to the derivative obtained in turbulent-free flow than the effective derivative obtained over several cycles of the model in turbulent flow.

The Reynolds numbers in the tunnel tests were roughly one-half those in the flight tests. The investigation of reference 8 showed that at Reynolds numbers of the order of 1×10^6 a reduction in Reynolds number caused a decrease in the damping-in-pitch derivative at subsonic speeds of a wing-body combination which had a 45° triangular wing with an NACA 0006-63 airfoil section.

The main effect of the difference in the shape of the support body would probably show up as a small modification in the direction of the flow at the tail. In the tunnel tests, the horizontal tail had one degree of freedom; in the flight tests, this condition was approximated.

The damping data for the other configurations tested were not worked up except incompletely in the case of the horizontal tail mounted on the sweptforward vertical tail. These data (not presented herein) showed an increase in magnitude of the static pitching-moment derivative $C_{m_{i_h}}$ with Mach number somewhat greater than that for the basic configuration, and a loss in damping at transonic speeds quite similar to that of the basic configuration. There was some indication that the loss in damping of the configuration with the sweptforward vertical tail developed at Mach numbers somewhat lower than those for the basic configuration. The loss in damping of the horizontal tail at transonic speeds appeared to be mainly a characteristic of the horizontal tail itself. The large-amplitude oscillations of the horizontal tail observed for the basic configuration at low supersonic Mach numbers (fig. 11(c)), however, were not observed for the configuration with the sweptforward vertical tail. It is concluded from these results that the vertical tail of the basic configuration with its associated interference effects was primarily responsible for the large-amplitude oscillations of the horizontal tail noted at low supersonic Mach numbers for the basic configuration, and that contributing factors were probably the loss in damping of the horizontal tail at transonic speeds and the turbulence of the airstream itself.

Horizontal-Tail Incidence at Trim Conditions

Plots of the mean trim angle of the horizontal tail against Mach number for the various configurations are shown in figures 18 to 20, inclusive. These data were obtained from cathetometer measurements. Trim data obtained from the oscillograph records showed the same trends with Mach number but were displaced somewhat in magnitude. The oscillograph trim data are not presented herein because the calibration of this instrument (in combination with the slide-wire indicator) proved to be somewhat unreliable.

Figure 18 presents flight and tunnel trim data for the horizontal tail of the basic configuration. The tunnel data for the basic configuration are averaged values from three separate runs. The symbol α used in figure 18 was the angle of attack of the tail support body in the flight tests. Also shown in figure 18 are trim data for the basic configuration less the canard servoplane from the tunnel tests. It is seen that the trim data from the tunnel tests for the basic configuration decreased gradually at subsonic speeds and rather abruptly at speeds just above a Mach number of 1. The tunnel results at a Mach number of 0.70 were essentially the same as those obtained in the flight tests at an angle of attack of 0°. The variation with Mach number, however, was different. The flight data showed no change in trim up to a Mach number of 0.9, and then showed an increase in trim at Mach numbers above 0.9. The increase amounted to approximately 1° between Mach numbers of 0.9 and 1.11. Unpublished flight data at an angle of attack of 5° and a canard deflection of 0° (fig. 18) showed a variation of trim with Mach number which was quite similar to that shown by the tunnel tests up to low supersonic Mach numbers. At supersonic Mach numbers above 1.05, the flight data at an angle of attack of 5° showed an increase in trim with Mach number similar to that shown by the flight data at an angle of attack of 0°. These flight results indicate that at small angles of attack and at Mach numbers near 1, the direction of the variation of trim with Mach number was sensitive to angle-of-attack changes. This sensitivity to angle of attack was shown in reference 1 by a considerable increase in the rate of change of trim angle of the horizontal tail with angle of attack at transonic speeds. For example, the rate of change of trim angle with angle of attack was approximately ten times as great at a Mach number of 1.1 as at a Mach number of 0.95.

As pointed out previously in the subsection entitled "Flow Angularity," the effective angle of attack of the horizontal tail in the tunnel tests was approximately 0.4° when the angle of attack α_b of the 3° conical support body was 0° and when the incidence of the horizontal tail i_h was 0°. The differences in the Mach number effects on trim between the tunnel tests and those of reference 1 may be explained at least partly in terms of angle-of-attack differences, even though the angle-of-attack differences (considering the accuracy of the flight and tunnel measurements) were probably no greater than 1° at the maximum.

Differences in the leading edge of the vertical tail adjacent to and within the horizontal tail in the flight and wind-tunnel configurations as discussed in the subsection entitled "Damping Characteristics," differences in test technique, Reynolds number, and model support may also have had an effect on the trim results.

The main effect of removal of the canard servoplane on the trim of the horizontal tail of the basic configuration showed up as a large decrease in trim at Mach numbers less than approximately 0.9 (fig. 18). This large decrease in trim indicates that at Mach numbers less than approximately 0.9 the canard servoplane on the basic configuration in effect carried a positive lift load at deflections of both 1° and -2°; it appears that the effects at these Mach numbers were primarily associated with the interference effects of the vertical tail of the basic configuration since corresponding trim changes were not obtained for the configuration with the sweptforward vertical tail on removal of the canard servoplane (fig. 20).

The addition of the image fins to the horizontal tail of the basic configuration reduced the variation of trim with Mach number at subsonic speeds and generally increased the trim angle (fig. 19). These changes were presumably a result of an opposing interference effect due to the fins and of the moment effect of the drag force on the fins. The rather abrupt trim changes at Mach numbers somewhat greater than 1 noted for the basic configuration (fig. 18) were also characteristic of the configurations with the image fins (fig. 19).

The trim changes at Mach numbers somewhat greater than 1 observed on the basic configuration (fig. 18) were not evident, however, when the horizontal tail was mounted on the small-chord sweptforward vertical tail (fig. 20). There was also a general increase in trim with Mach number at subsonic speeds instead of the decrease observed for the basic configuration. The trim changes of the basic configuration appeared to be modified by the vertical tail of the basic configuration and its associated interference effects, in addition to the modification resulting from the increased sensitivity of the trim angle to angle of attack at transonic speeds as found in the flight tests.

The effectiveness of the canard servoplane on the basic configuration as determined from flight and tunnel tests is presented in figure 21. The flight results are unpublished data at an angle of attack of 0°. Flight-effectiveness data are also given in reference 1, but those data are for an angle of attack which was only approximately 0°, and subsequent flight investigation and analysis have shown that the effectiveness was quite sensitive to angle-of-attack changes. The flight and tunnel effectiveness results of figure 21 show the same trends with Mach number, with the tunnel values being somewhat lower than the flight values. The effectiveness of the canard servoplane on the configuration with the sweptforward

vertical tail (data not shown) was approximately 0.17 and was essentially invariant with change in Mach number.

Local Mach Numbers and Schlieren Photographs

Surface Mach number distributions along the 3° conical support body and on the vertical tail of the basic configuration and schlieren photographs of the flow are shown in figures 22 to 27, inclusive, for the various configurations for a canard servoplane deflection of 1°. The schlieren and pressure data at a canard servoplane deflection of -2° (not presented herein) were essentially the same as those for a deflection of 1°. Schlieren data were obtained over an incomplete Mach number range at the boom base for the basic configuration (fig. 22(c)). The shock formations at the boom base for the basic configuration, however, would be expected to be similar to those shown in figure 23(b) for the basic configuration less the canard servoplane.

The schlieren survey was not sufficiently complete to identify all the shock waves evident in the photographs. The shock wave (a) shown in figure 22(b) originated from the juncture of the 3° conical support body and the leading edge of the vertical tail of the basic configuration. The reflection of shock (a) off the lower boundary of the tunnel is evident as shock (a') in figures 23(b) and 25(b). It is apparent that even at the highest Mach number, the reflected shock (a') did not appear to be completely free of influencing the flow over the model. The origin of shock (a) was located off the center line of the tunnel (fig. 4), however, so that the reflected wave from the tunnel boundaries had a nonfocusing effect on the model. The interference effect of the reflected wave in such a case could be expected to be somewhat less than had the shock originated at the tunnel center line (ref. 3). Figure 22(b) indicates that the shock (a) and the bow wave (b) off the canard servoplane merged above the model. The reflection of these waves off the upper boundary of the tunnel would be expected to clear the model at the highest speeds. The shock (a") in figure 22(b) is apparently the shock wave (a) striking the windows in the tunnel boundary.

The shock (c) shown in figures 23(b), 25(b), 26(b), and 27(b) is probably a model shock striking the tunnel windows. Replacement of the vertical tail of the basic configuration by the sweptforward vertical tail still showed the same general shock patterns but lowered the Mach numbers by roughly 0.04 or 0.05 at which the shock phenomena, such as the inclined shocks at the trailing-edge and hinge-axis regions of the stabilator, appeared. This shift in the shock patterns to lower Mach numbers appeared to be accompanied by a corresponding shift to lower Mach numbers of the development of the loss in damping derivative at transonic speeds.

CONCLUDING REMARKS

An investigation was made in the Langley 8-foot transonic tunnel of the trim and dynamic response characteristics of the free-floating horizontal tail of a 1/7-scale model of the complete tail of the Grumman XF10F-1 airplane. Additional tests were made with the horizontal tail supported on an auxiliary small-chord sweptforward vertical tail. The tests were made at Mach numbers up to 1.13. The following concluding statements are indicated:

1. A loss in damping of the horizontal tail at transonic speeds occurred with the horizontal tail mounted on either the vertical tail of the basic configuration or the auxiliary sweptforward vertical tail.

2. The damping characteristics of the horizontal tail of the basic configuration as determined from tunnel and flight tests showed the same general trends with Mach number. The static pitching-moment derivative of the horizontal tail $C_{m_{i_h}}$ increased with Mach number at a greater rate in the tunnel tests. The damping derivative of the horizontal tail $C_{m_{\dot{i}_h}}$ was less in the tunnel tests, and the loss in damping at transonic speeds extended over a greater Mach number range and the maximum loss occurred at a higher Mach number in the tunnel tests.

3. Large-amplitude oscillations of the horizontal tail of the basic configuration occurred at low supersonic Mach numbers. The vertical tail of the basic configuration and the interference effects associated with this tail appeared to be primarily responsible for these characteristics; secondary factors probably were the loss in damping of the horizontal tail at transonic speeds and the turbulence of the airstream itself.

Langley Aeronautical Laboratory,
National Advisory Committee for Aeronautics,
Langley Field, Va.

Arvo A. Luoma

Arvo A. Luoma
Aeronautical Research Scientist

Approved:

Eugene C. Draley

Eugene C. Draley
Chief of Full Scale Research Division

ecc

REFERENCES

1. Gardner, William N., and Edmondson, James L.: Preliminary Results Obtained From Flight Test of a Rocket Model Having the Tail Only of the Grumman XF10F Airplane Configuration - TED No. NACA DE 354. NACA RM SL51E04, Bur. Aero., 1951.

2. Wright, Ray H., and Ward, Vernon G.: NACA Transonic Wind-Tunnel Test Sections. NACA RM L8J06, 1948.

3. Ritchie, Virgil S., and Pearson, Albin O.: Calibration of the Slotted Test Section of the Langley 8-Foot Transonic Tunnel and Preliminary Experimental Investigation of Boundary-Reflected Disturbances. NACA RM L51K14, 1952.

4. Wright, Ray H., and Ritchie, Virgil S.: Characteristics of a Transonic Test Section With Various Slot Shapes in the Langley 8-Foot High-Speed Tunnel. NACA RM L51H10, 1951.

5. Whitcomb, Charles F., and Osborne, Robert S.: An Experimental Investigation of Boundary Interference on Force and Moment Characteristics of Lifting Models in the Langley 16- and 8-Foot Transonic Tunnels. NACA RM L52L29, 1953.

6. Cahill, Jones F., and Bird, John D.: Low-Speed Tests of a Free-to-Yaw Model in Two Wind Tunnels of Different Turbulence. NACA RM L51L14, 1952.

7. Bird, John D.: Some Calculations of the Lateral Response of Two Airplanes to Atmospheric Turbulence With Relation to the Lateral Snaking Problem. NACA RM L50F26a, 1950.

8. Tobak, Murray, Reese, David E., Jr., and Beam, Benjamin H.: Experimental Damping in Pitch of 45° Triangular Wings. NACA RM A50J26, 1950.

TABLE I.- SPECIFICATIONS OF 1/7-SCALE MODEL OF COMPLETE TAIL

OF GRUMMAN XF10F-1 AIRPLANE

Horizontal tail:	
Main lifting surface of horizontal tail:	
Airfoil section	Grumman special
Thickness ratio	0.04
Aspect ratio	2
Taper ratio	0
Span, in.	20.6
Root chord, in.	20.6
Area (including stabilator), sq ft	1.47
Mean aerodynamic chord, in.	13.7
Dihedral, deg	0
Sweep angle, leading edge, deg	63.4
Stabilator:	
Chord, in.	2.17
Area, percent area of main lifting surface of horizontal tail	20
Location of hinge axis above plane of main lifting surface of horizontal tail, in.	0
Location of hinge axis from pivot axis of horizontal tail, in.	7.58
Canard servoplane:	
Airfoil section	Grumman special
Thickness ratio	0.06
Aspect ratio	2
Taper ratio	0
Span, in.	5.93
Root chord, in.	5.93
Area, sq ft	0.122
Mean aerodynamic chord, in.	3.95
Location of hinge axis above plane of main lifting surface of horizontal tail, in.	0.3
Location of hinge axis from pivot axis of horizontal tail, in.	17.47
Location of hinge axis from nose of canard servoplane, in.	3.85
Dihedral, deg	0
Sweep angle, leading edge, deg	63.4

NACA

TABLE I.- SPECIFICATIONS OF 1/7-SCALE MODEL OF COMPLETE TAIL

OF GRUMMAN XF10F-1 AIRPLANE - Concluded

Vertical tail:	
Airfoil section, parallel to center line of 3° conical support body	NACA 64A008
Sweep angle, leading edge, deg	59.1
Sweep angle, trailing edge, deg	28.5
Distance from center line of 3° conical support body to pivot axis of horizontal tail, in.	13.86

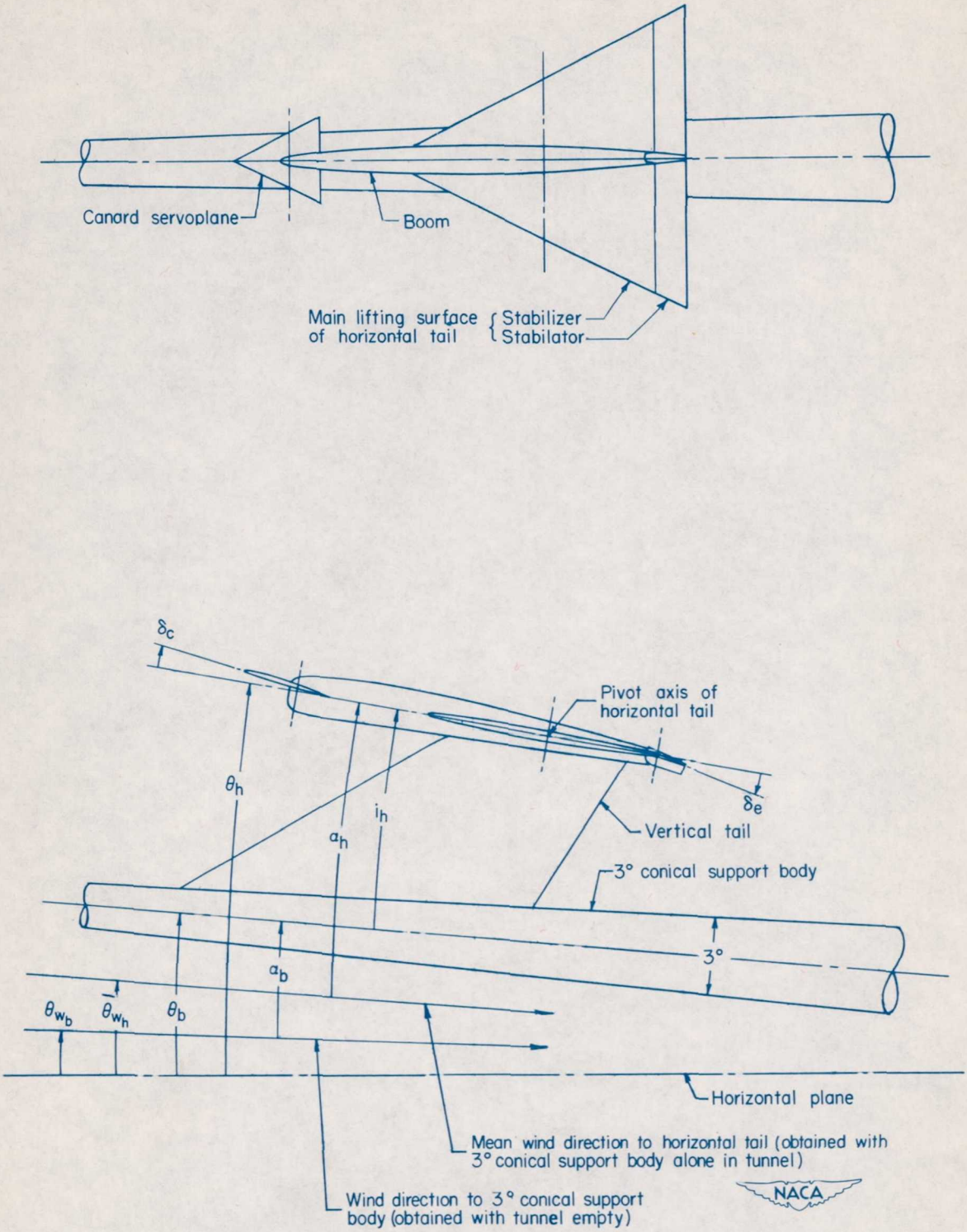

Figure 1.- General arrangement of 1/7-scale model of complete tail of Grumman XF10F-1 airplane mounted on 3° conical support body. Positive directions of angles shown.

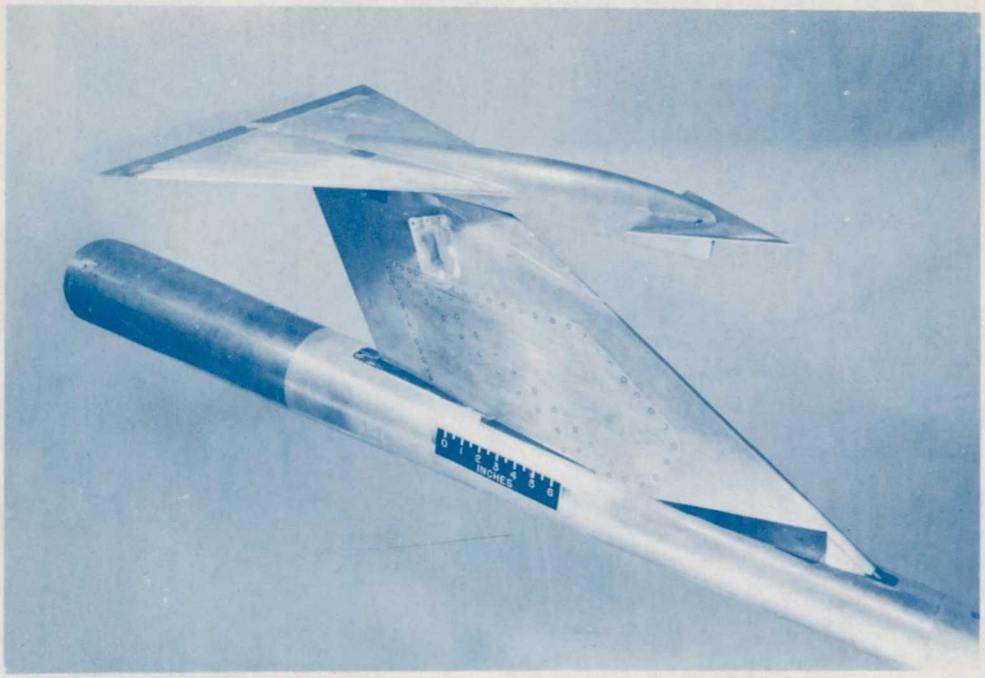

(a) Three-quarter front view. L-73185.1

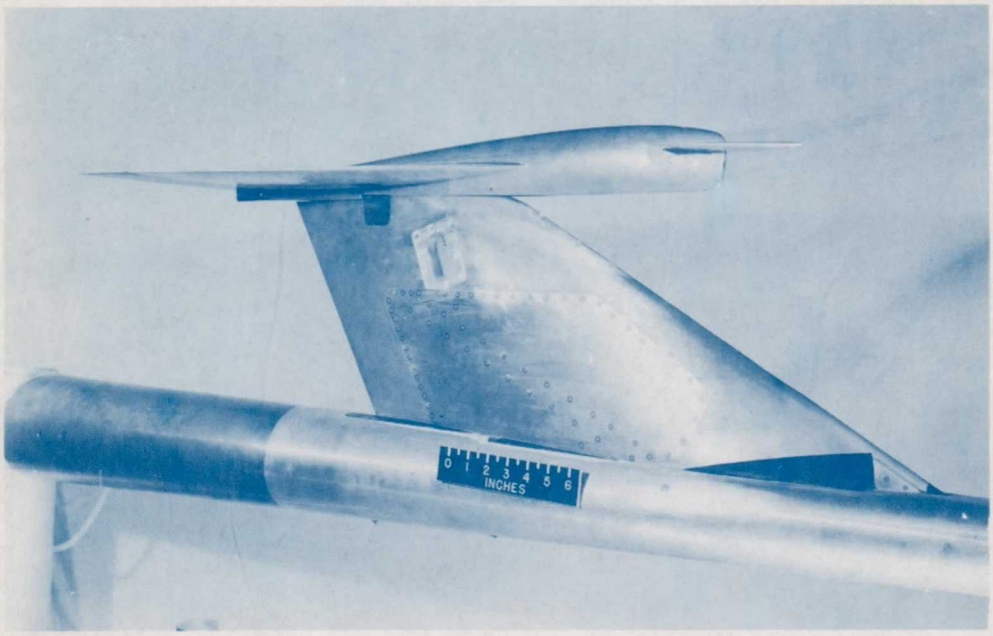

(b) Side view. L-73186

Figure 2.- Photograph of 1/7-scale model of complete tail of Grumman XF10F-1 airplane mounted on 3° conical support body.

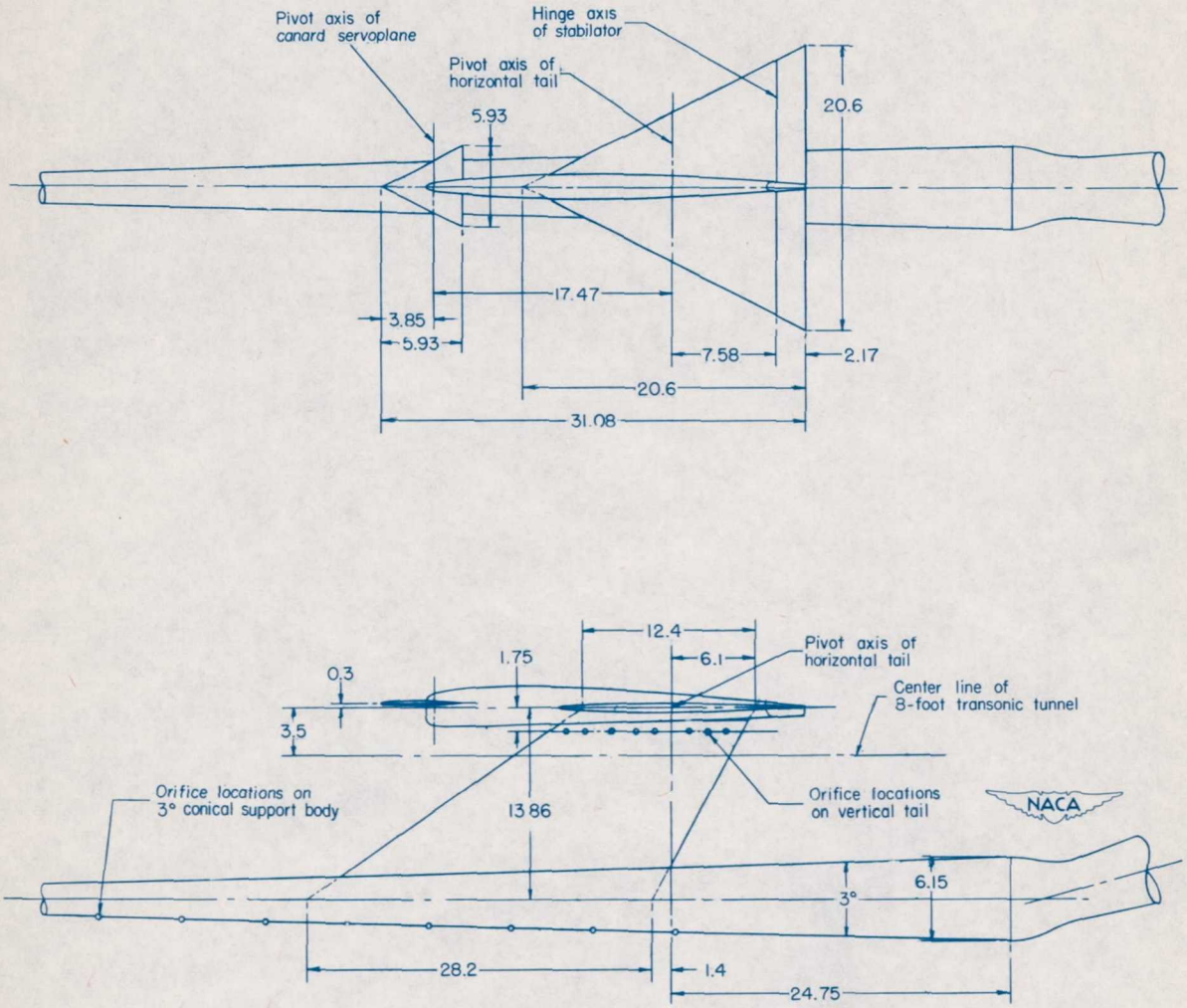

Figure 3.- Dimensions of 1/7-scale model of complete tail of Grumman XF10F-1 airplane mounted on 3° conical support body. All dimensions are in inches except as noted.

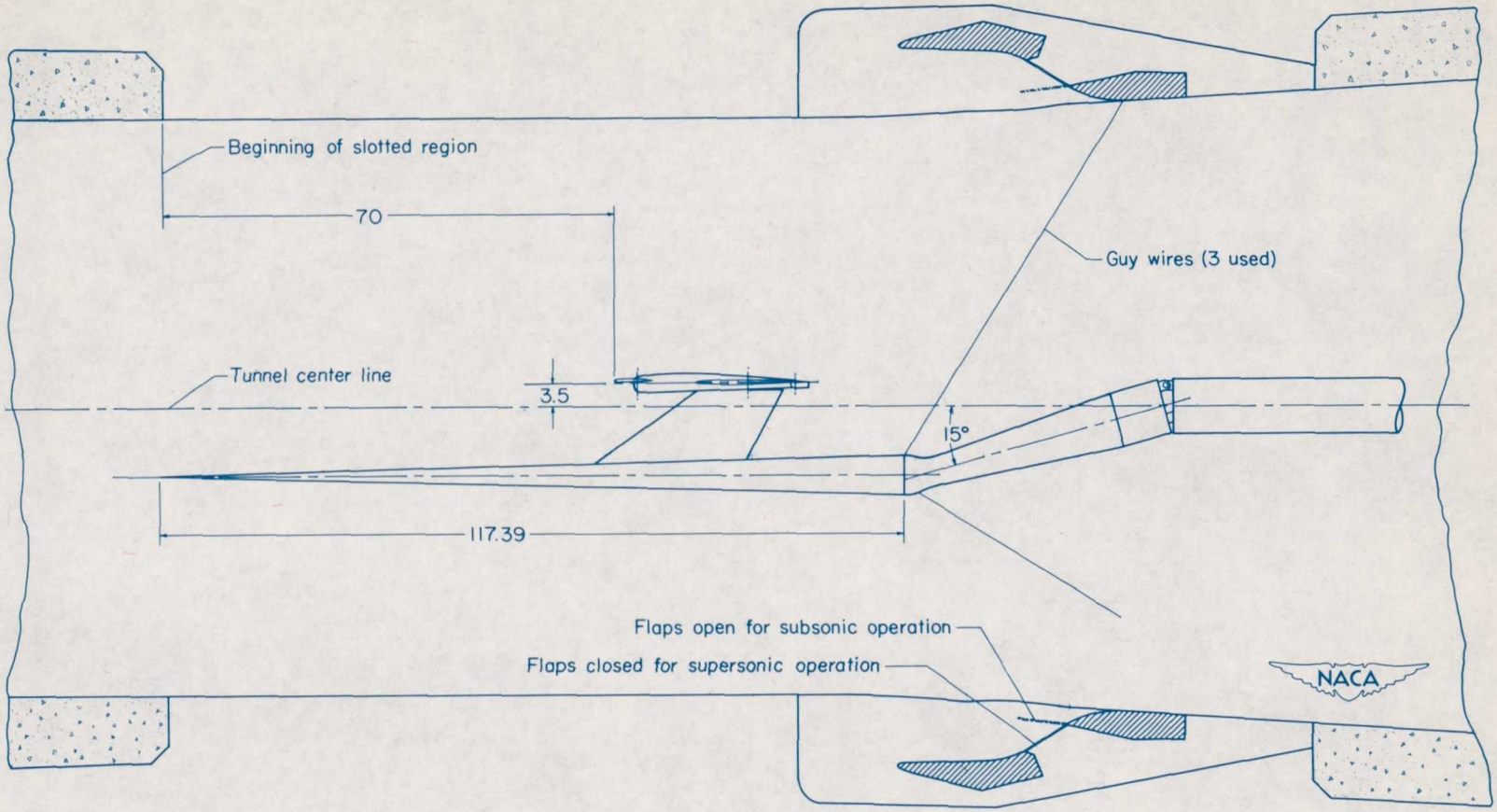

Figure 4.- Location of 1/7-scale model of complete tail of Grumman XF10F-1 airplane in slotted test section of Langley 8-foot transonic tunnel. All dimensions are in inches except as noted.

CONFIDENTIAL

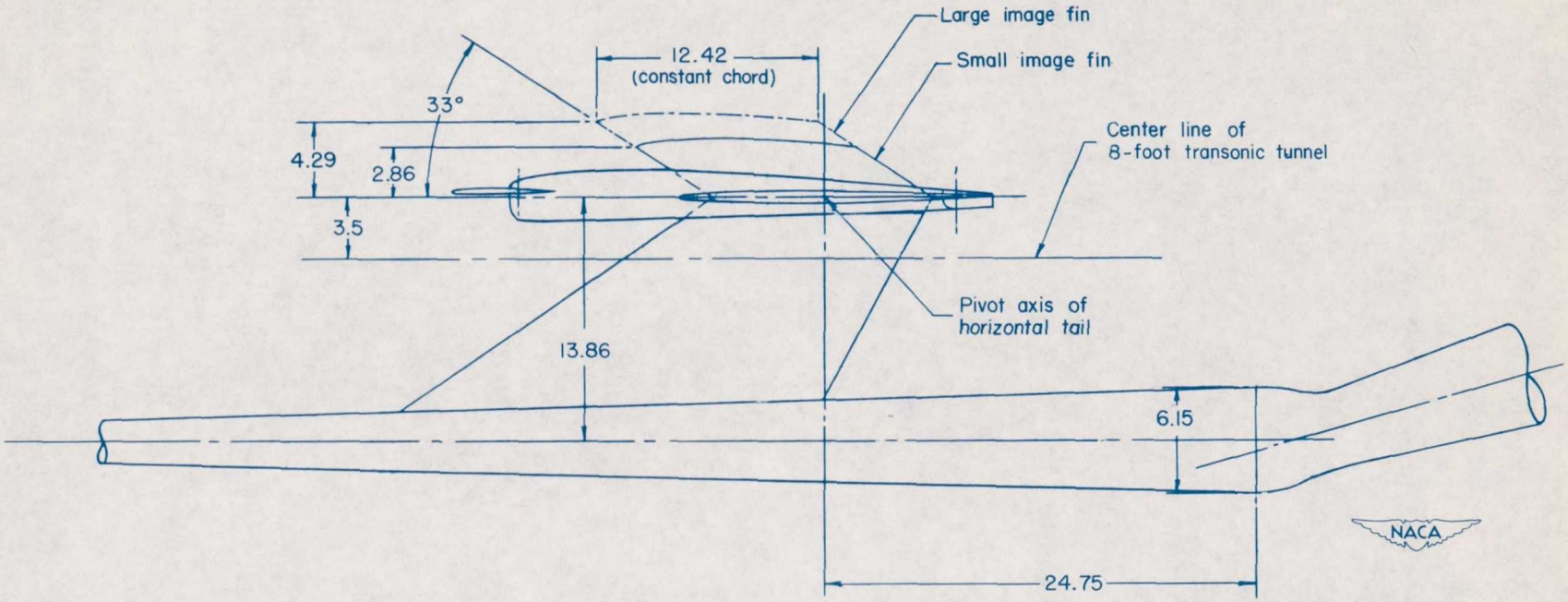

Figure 5.- Dimensions of 1/7-scale model of complete tail of Grumman XF10F-1 airplane in combination with image fin and mounted on 3° conical support body. All dimensions are in inches except as noted.

CONFIDENTIAL

CONFIDENTIAL

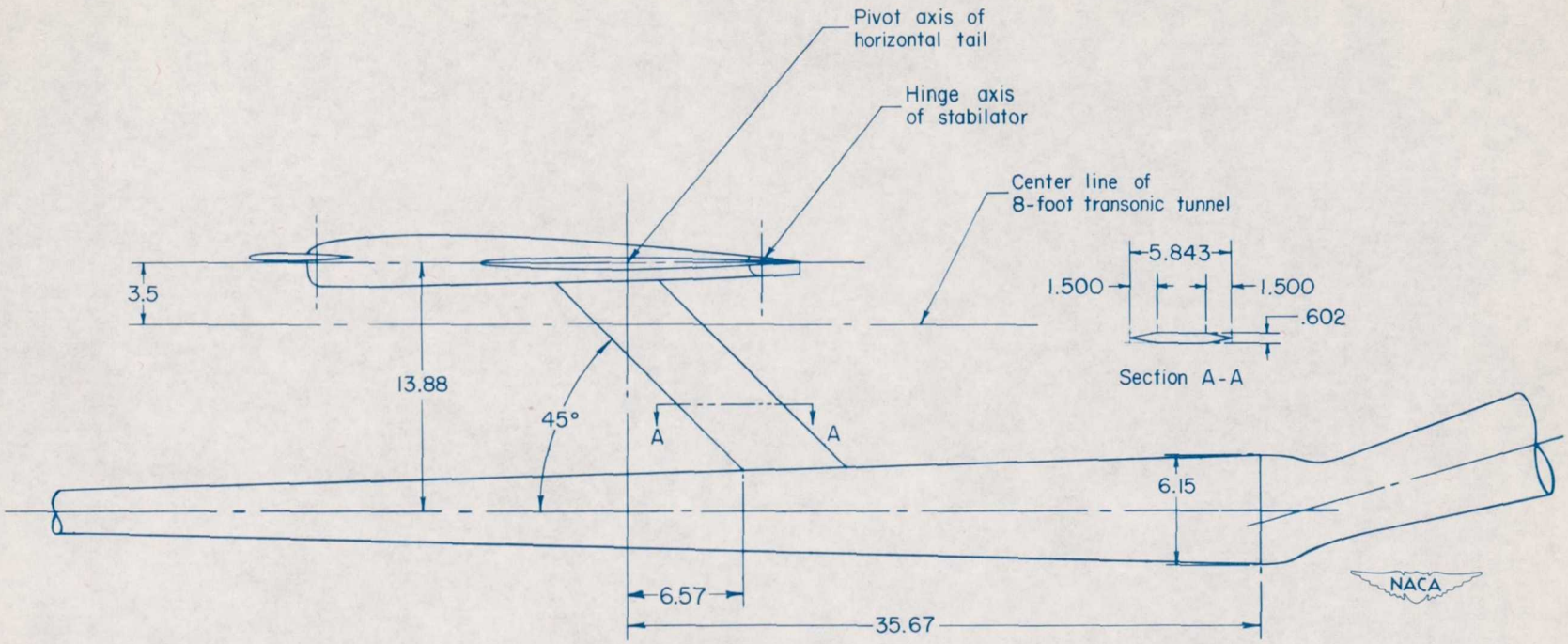

Figure 6.- Dimensions of 1/7-scale model of horizontal tail of Grumman XF10F-1 airplane in combination with auxiliary small-chord swept-forward vertical tail and mounted on 3° conical support body. All dimensions are in inches except as noted.

CONFIDENTIAL

(a) Three-quarter front view. L-73557

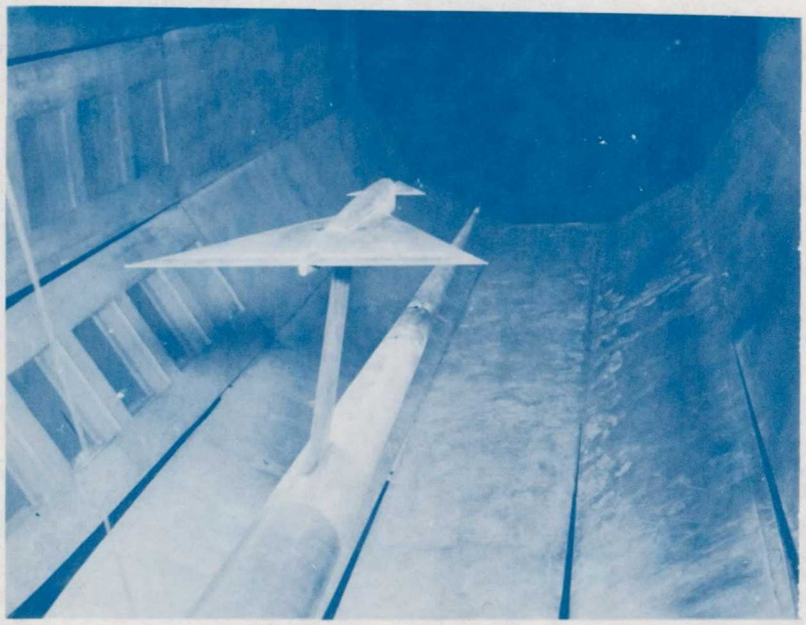

(b) Three-quarter rear view. L-73558

Figure 7.- Photograph of 1/7-scale model of horizontal tail of Grumman XF10F-1 airplane in combination with auxiliary small-chord swept-forward vertical tail and mounted on 3° conical support body in Langley 8-foot transonic tunnel.

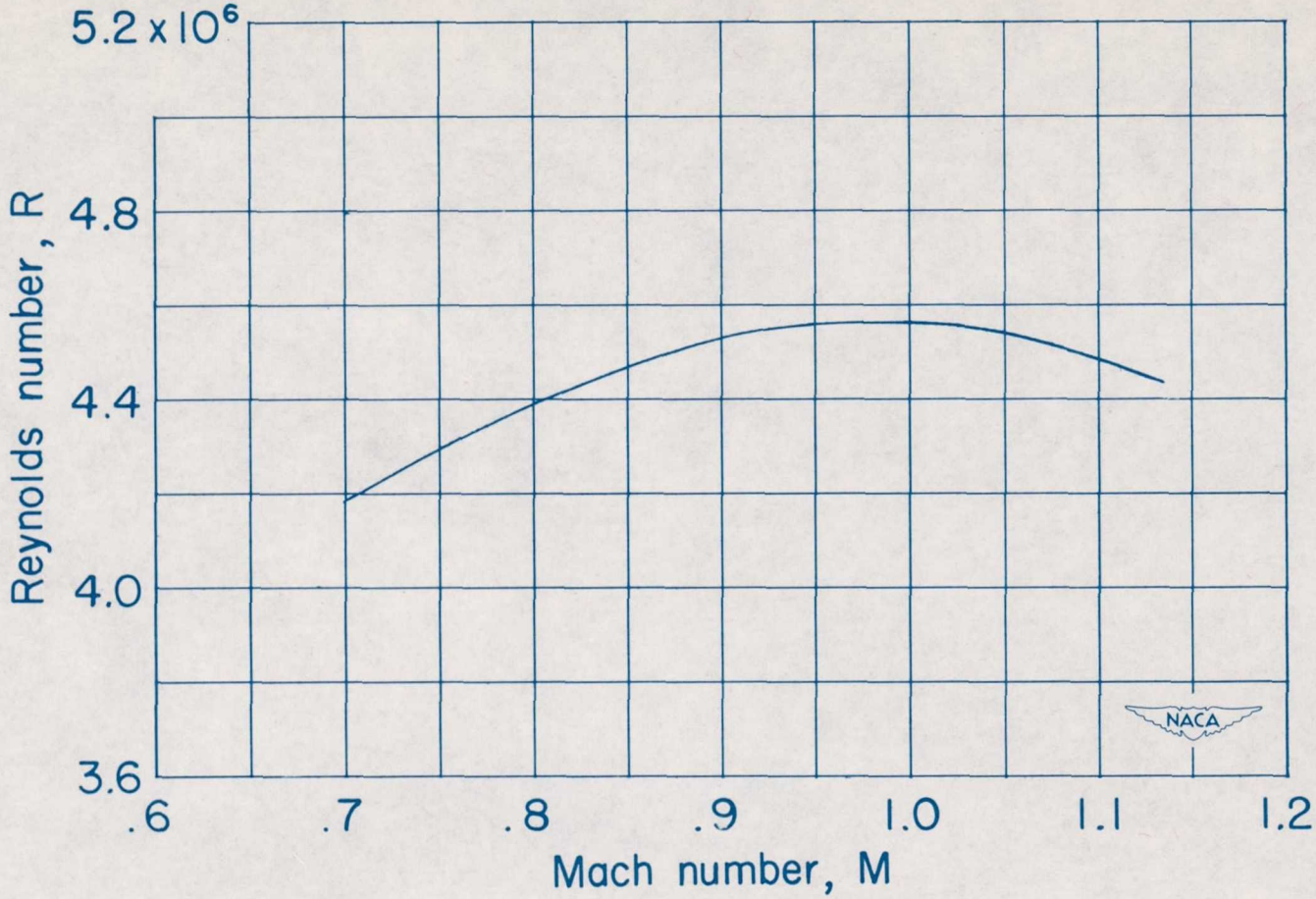

Figure 8.- Variation of Reynolds number (based on a mean aerodynamic chord of 13.7 inches) with Mach number in tests of 1/7-scale model of complete tail of Grumman XF10F-1 airplane in Langley 8-foot transonic tunnel.

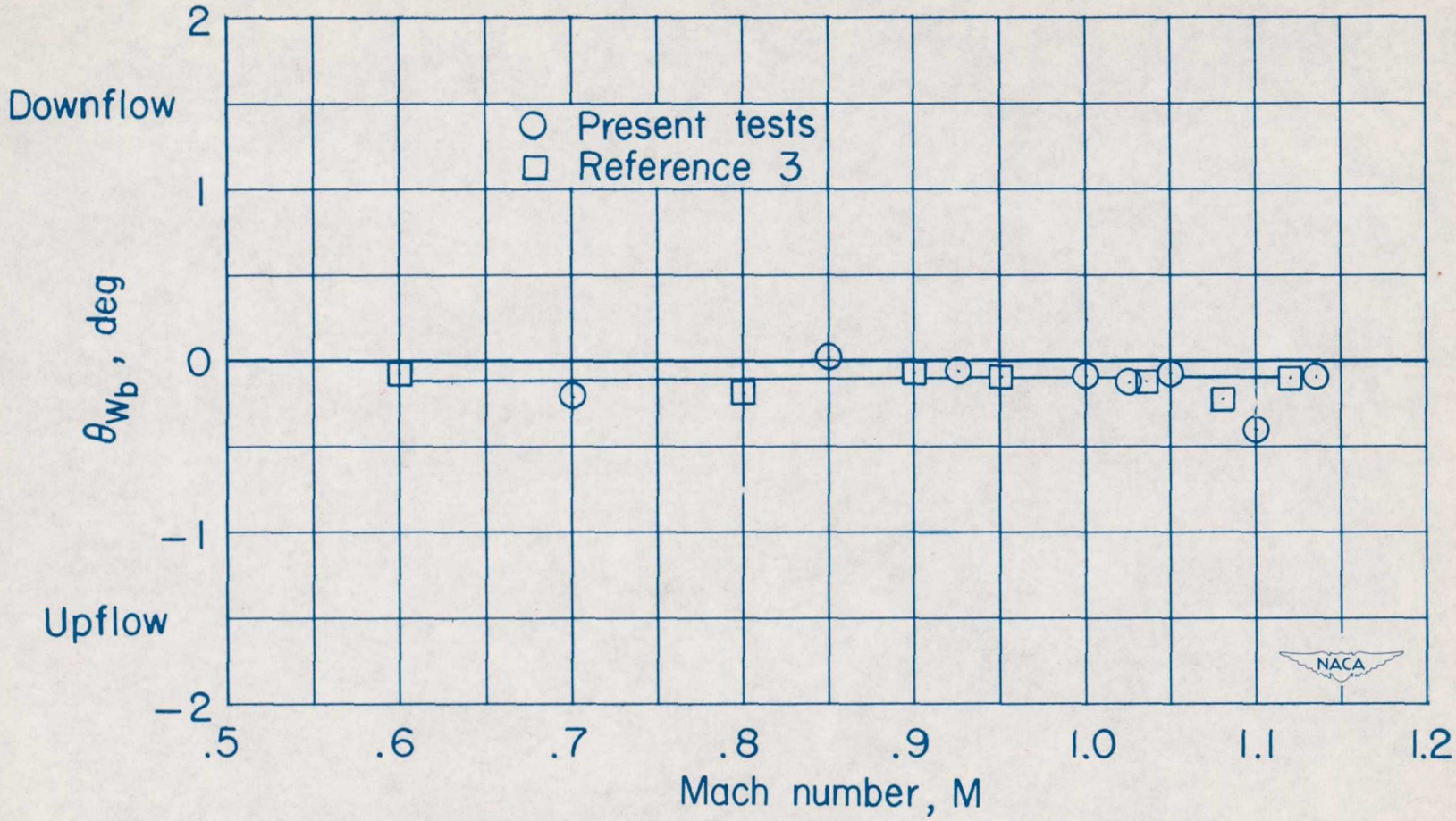

Figure 9.- Inclination (in vertical plane) of flow at center line of test section of Langley 8-foot transonic tunnel with no model in tunnel.

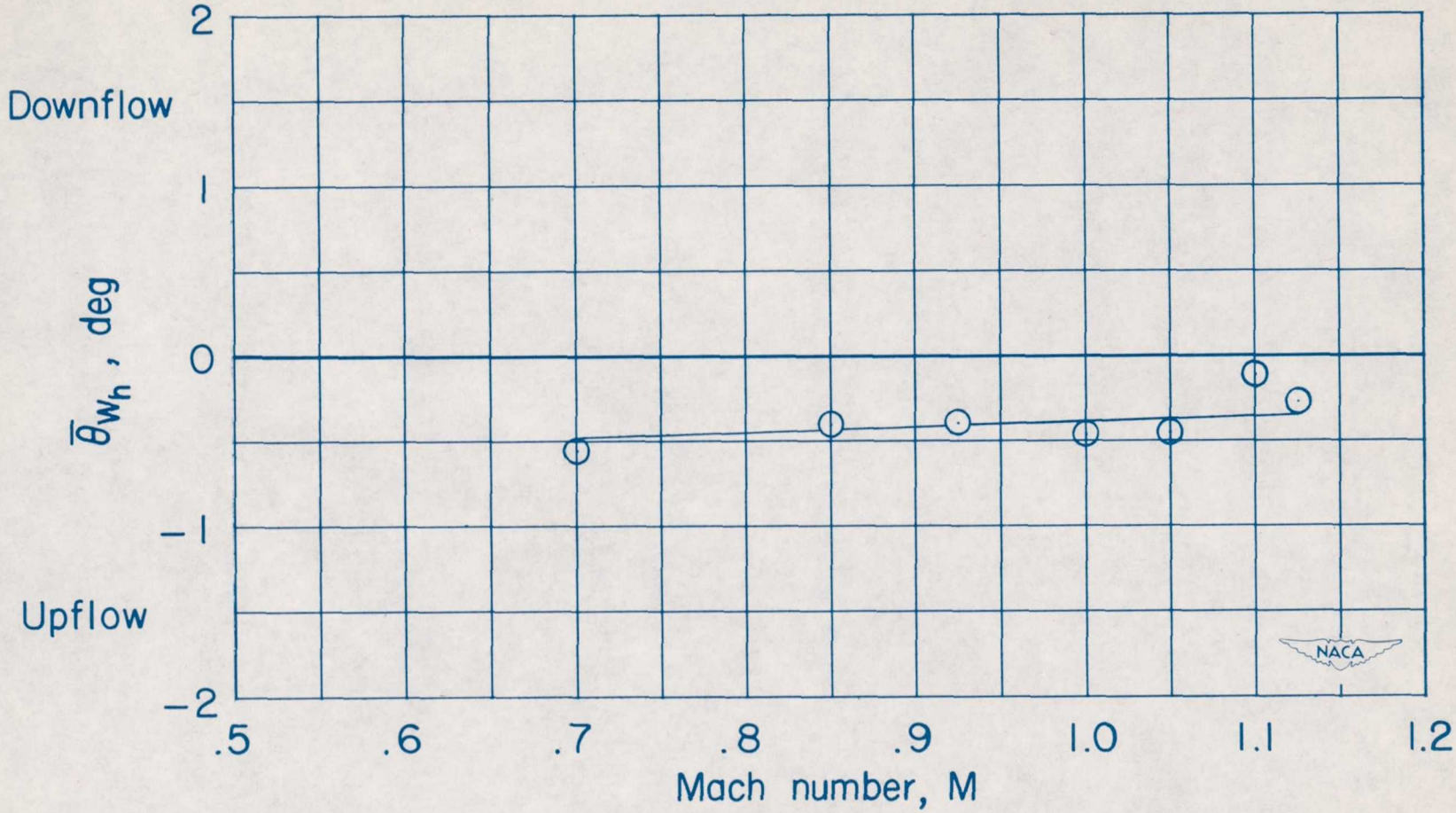

Figure 10.- Mean inclination (in vertical plane) of flow in region occupied by horizontal tail obtained with 3° conical support body alone in tunnel. $\alpha_b = 0^{\circ}$.

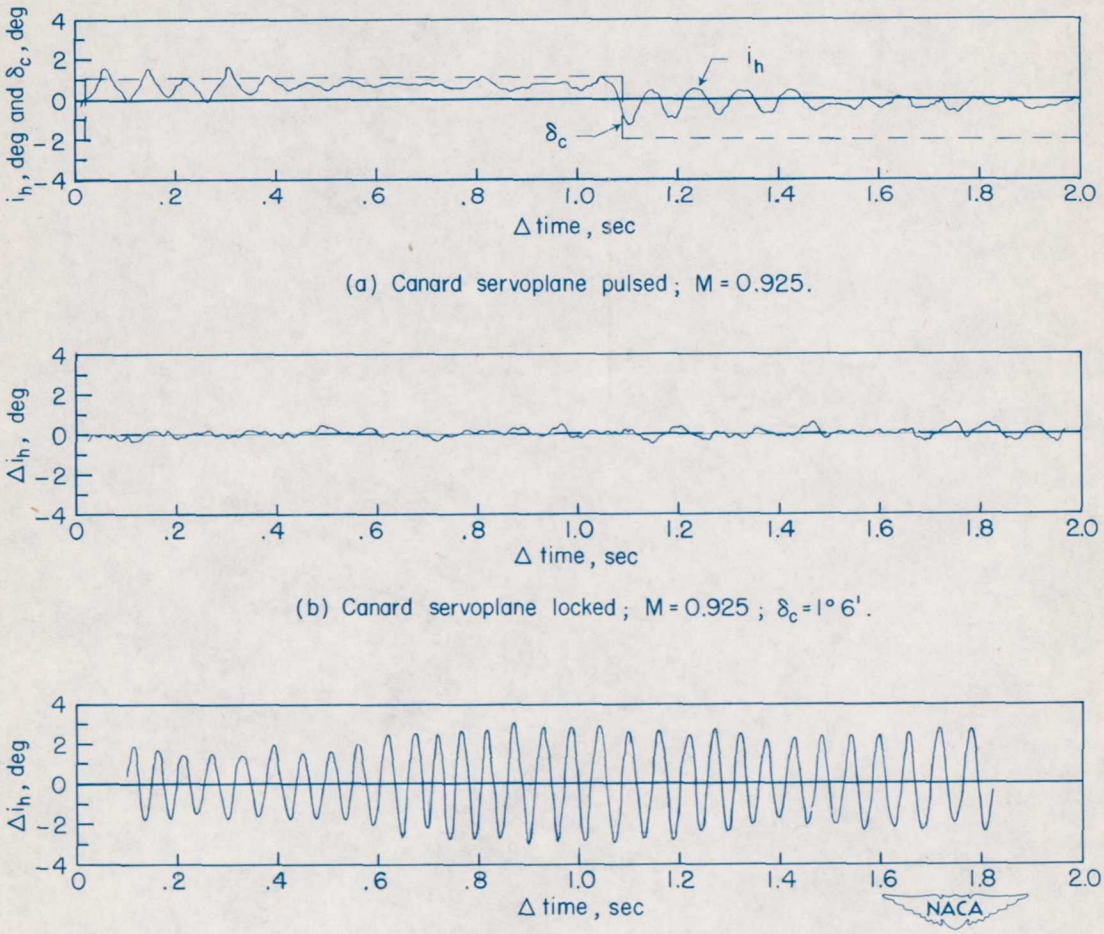

Figure 11.- Typical records of oscillations of horizontal tail for 1/7-scale model of complete tail of Grumman XF10F-1 airplane mounted on 3° conical support body in Langley 8-foot transonic tunnel.

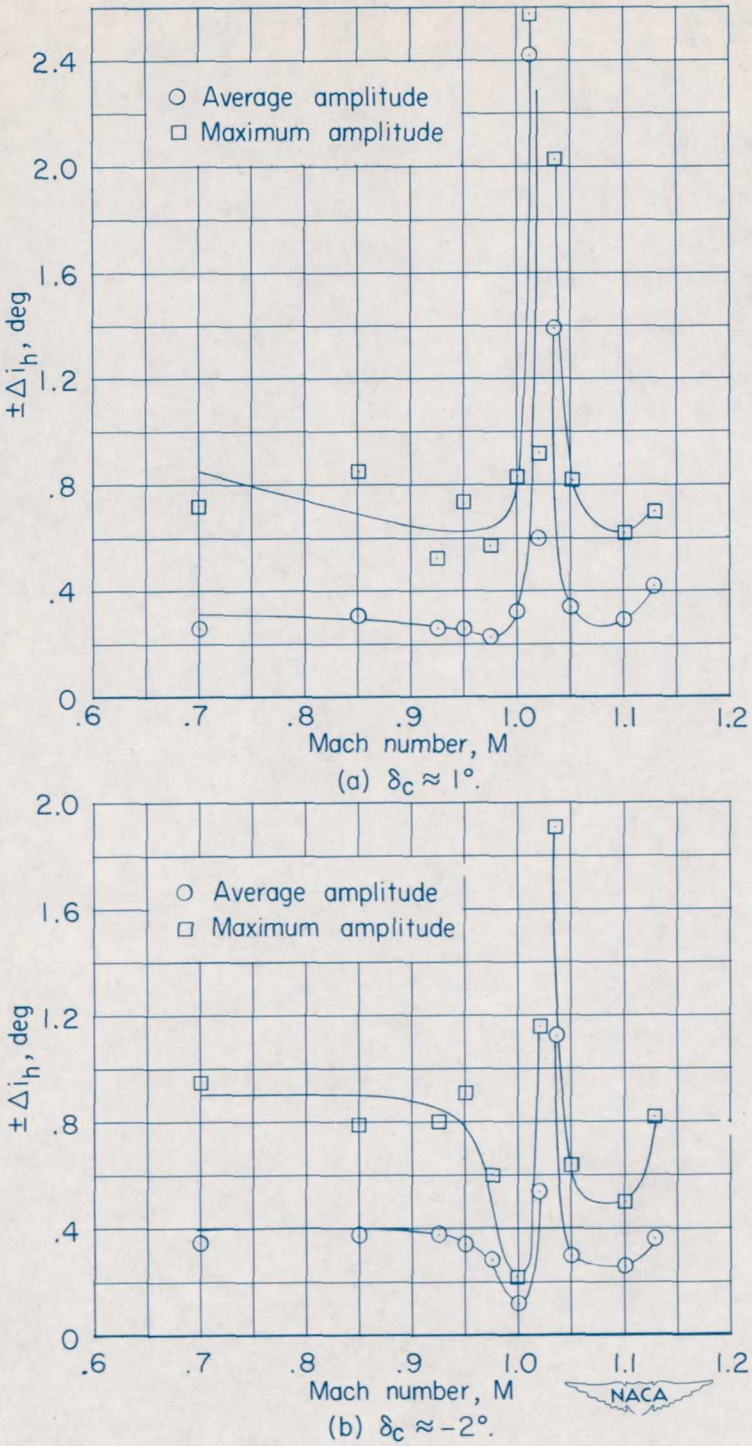

Figure 12.- Amplitude of oscillation (from mean trim position) of horizontal tail with canard servoplane locked for 1/7-scale model of complete tail of Grumman XF10F-1 airplane mounted on 3° conical support body in Langley 8-foot transonic tunnel. $\alpha_b = 0°$.

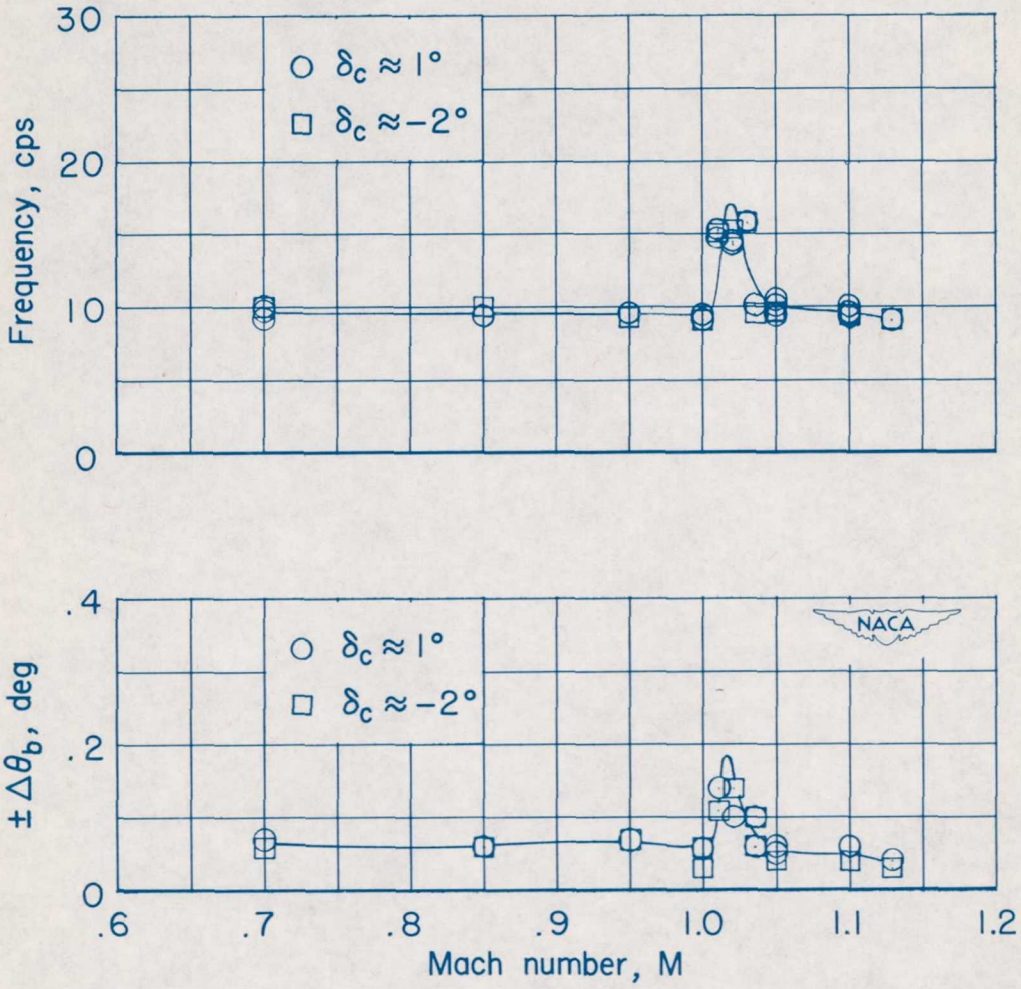

Figure 13.- Frequency and maximum amplitude (from mean position) of oscillation of 3° conical support body in combination with 1/7-scale model of complete tail of Grumman XF10F-1 airplane with canard servoplane locked, in Langley 8-foot transonic tunnel. $\alpha_b = 0°$.

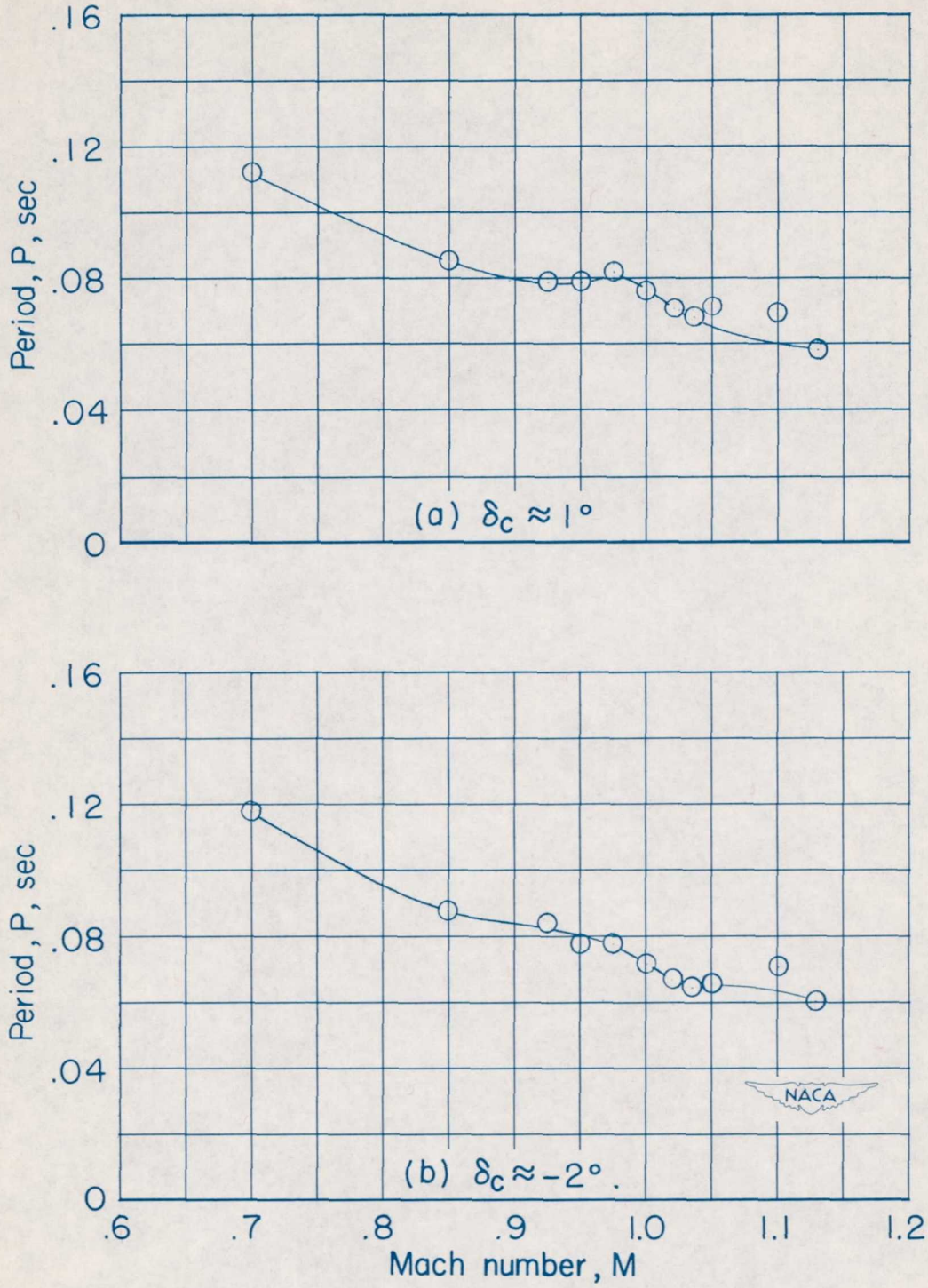

Figure 14.- Variation with Mach number of period of oscillation (following control pulse) of horizontal tail of 1/7-scale model of complete tail of Grumman XF10F-1 airplane mounted on 3° conical support body in Langley 8-foot transonic tunnel. $\alpha_b = 0°$.

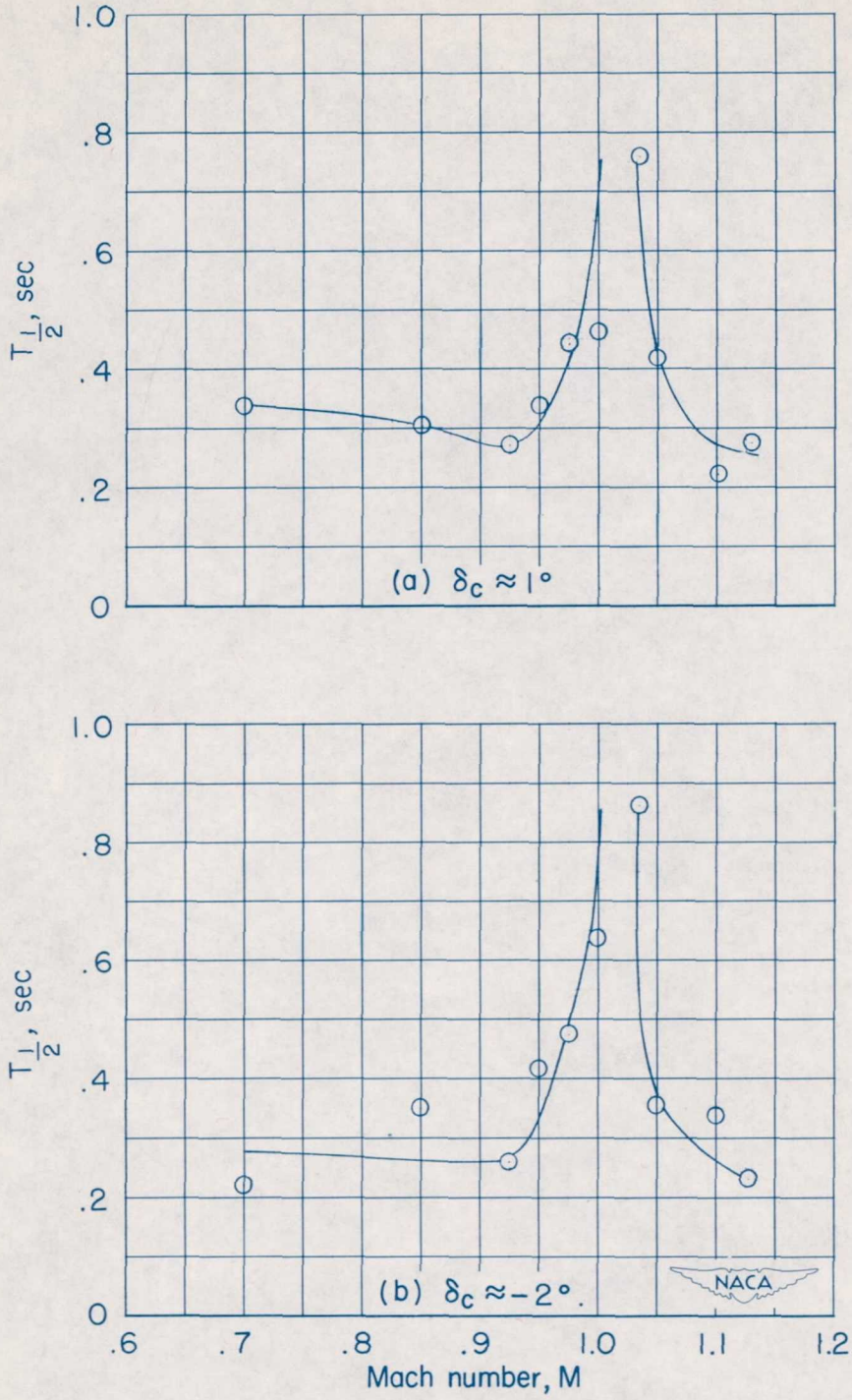

Figure 15.- Variation with Mach number of time to damp to one-half amplitude of oscillation (following control pulse) of horizontal tail of 1/7-scale model of complete tail of Grumman XF10F-1 airplane mounted on 3° conical support body in Langley 8-foot transonic tunnel. $\alpha_b = 0°$.

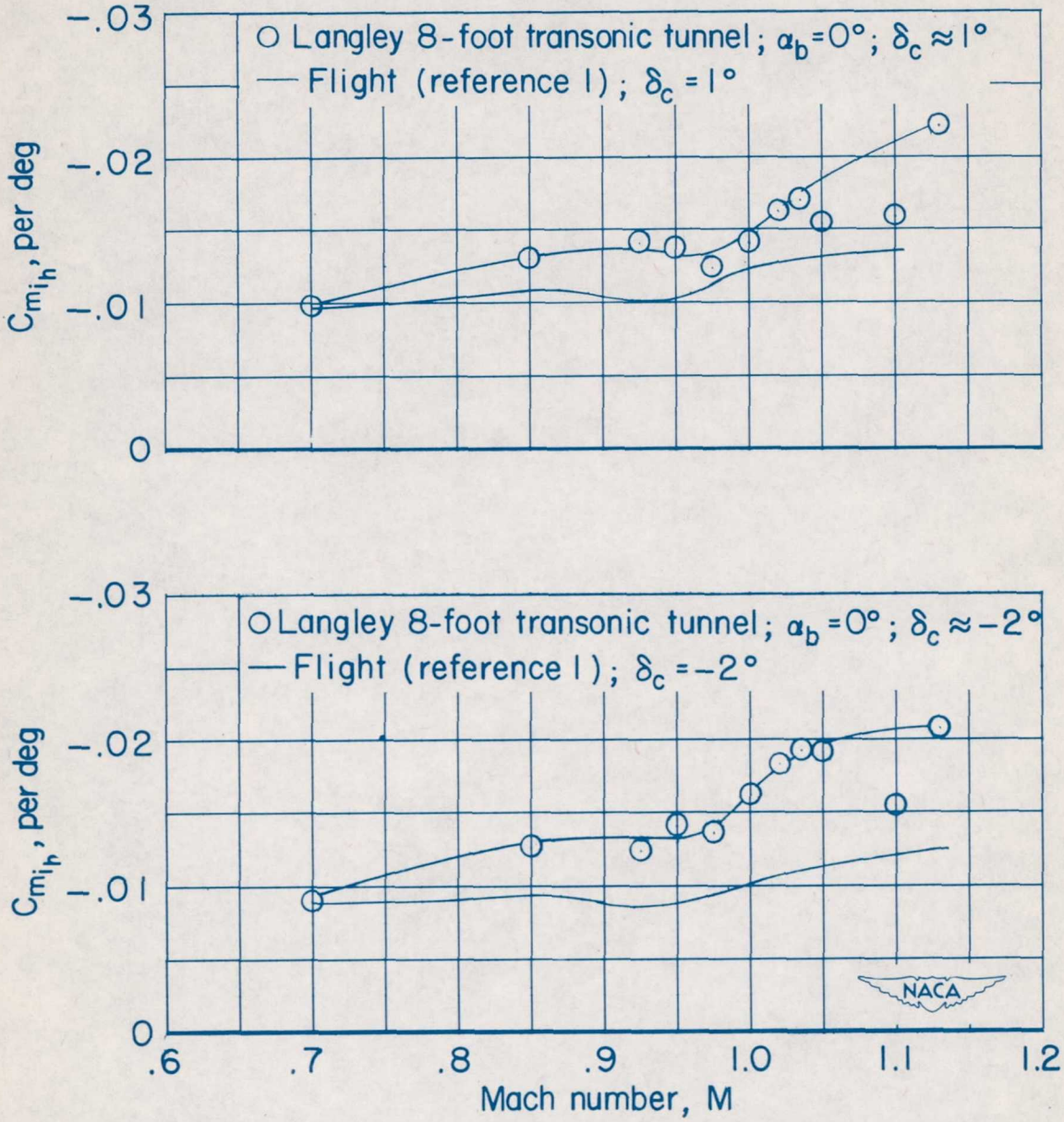

Figure 16.- Variation with Mach number of static pitching-moment derivative $C_{m_{i_h}}$ of horizontal tail of 1/7-scale model of complete tail of Grumman XF10F-1 airplane.

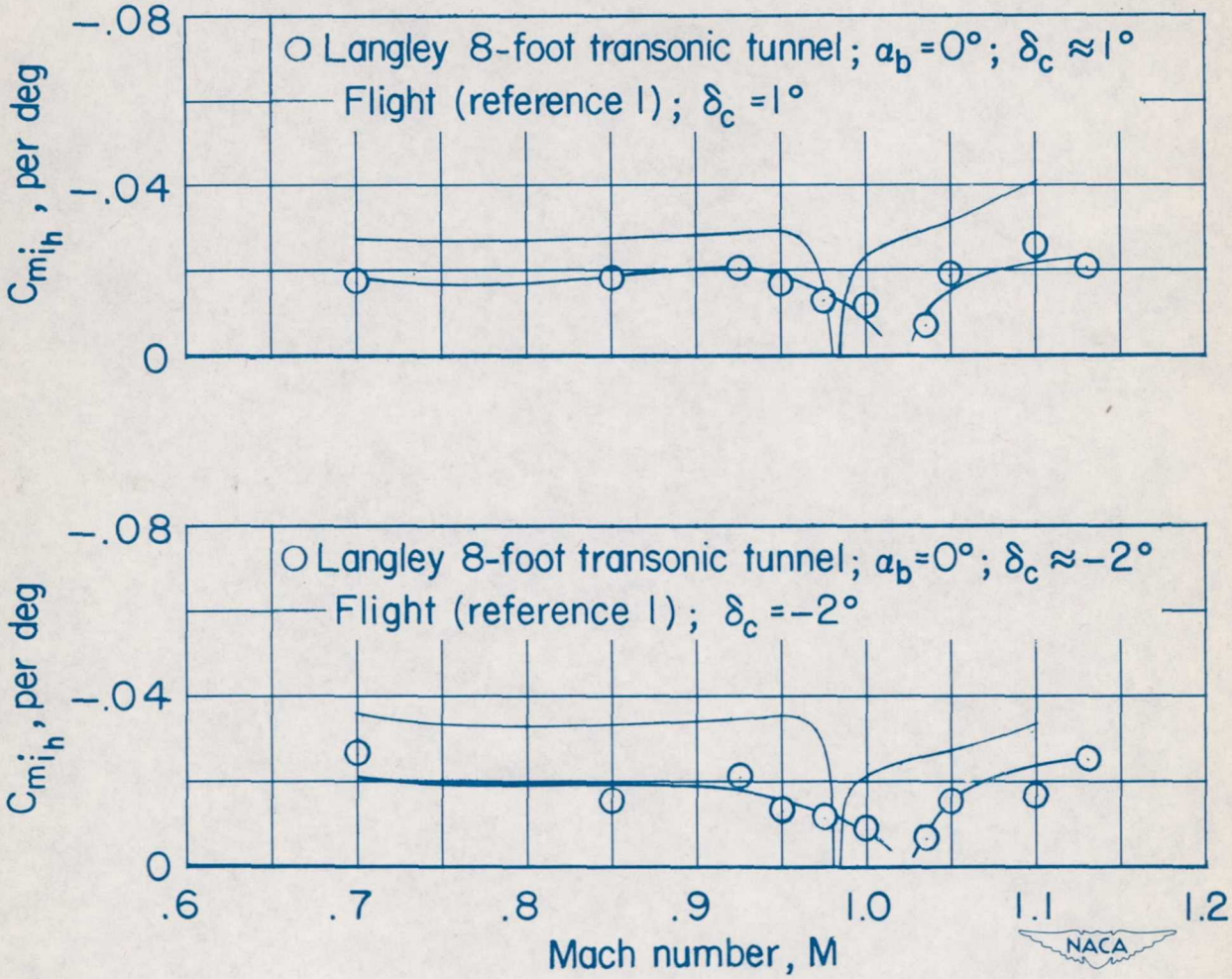

Figure 17.- Variation with Mach number of damping derivative $C_{m_{i_h}}$ of horizontal tail of 1/7-scale model of complete tail of Grumman XF10F-1 airplane.

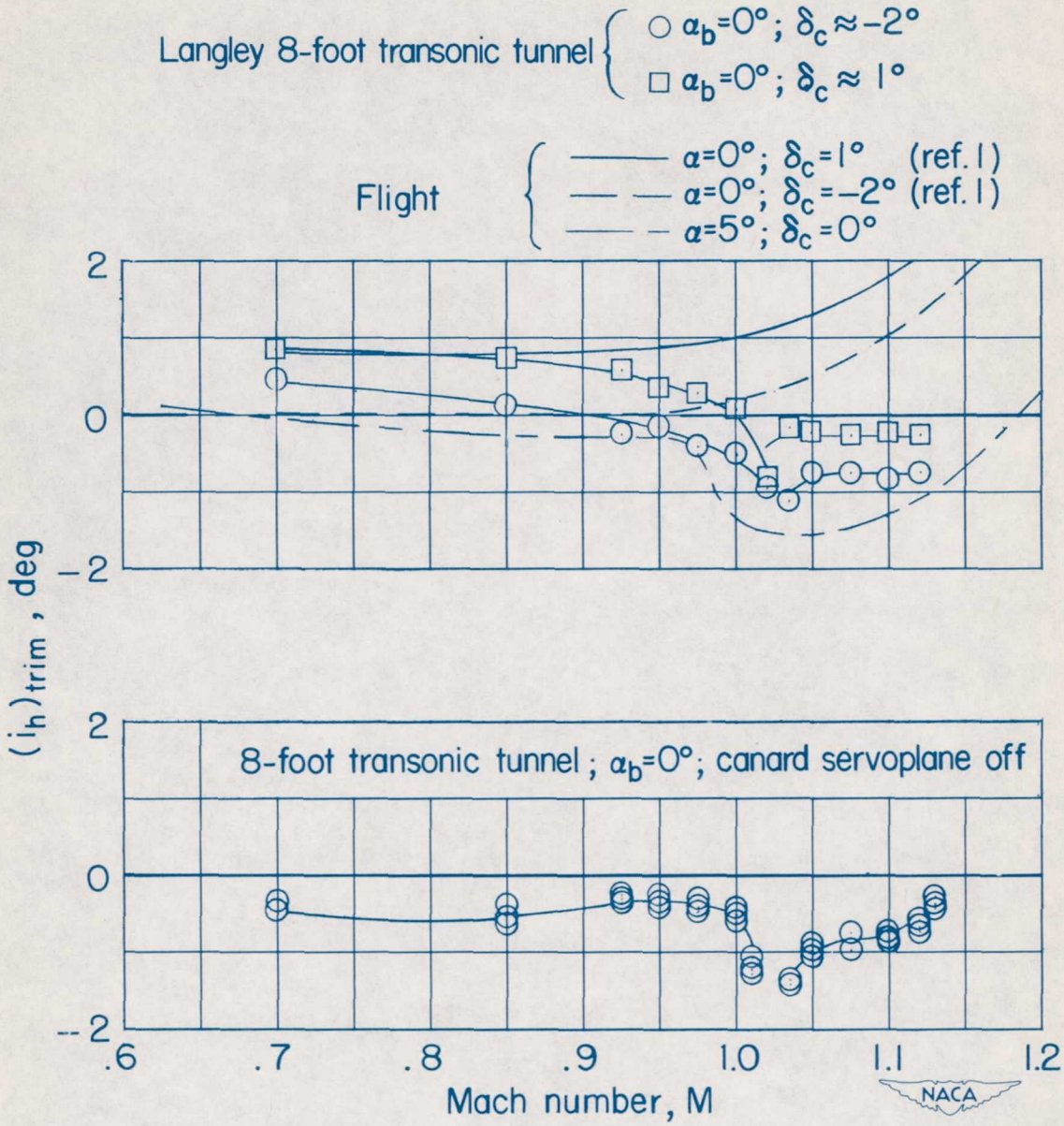

Figure 18.- Variation of floating angle of horizontal tail against Mach number for 1/7-scale model of complete tail of Grumman XF10F-1 airplane.

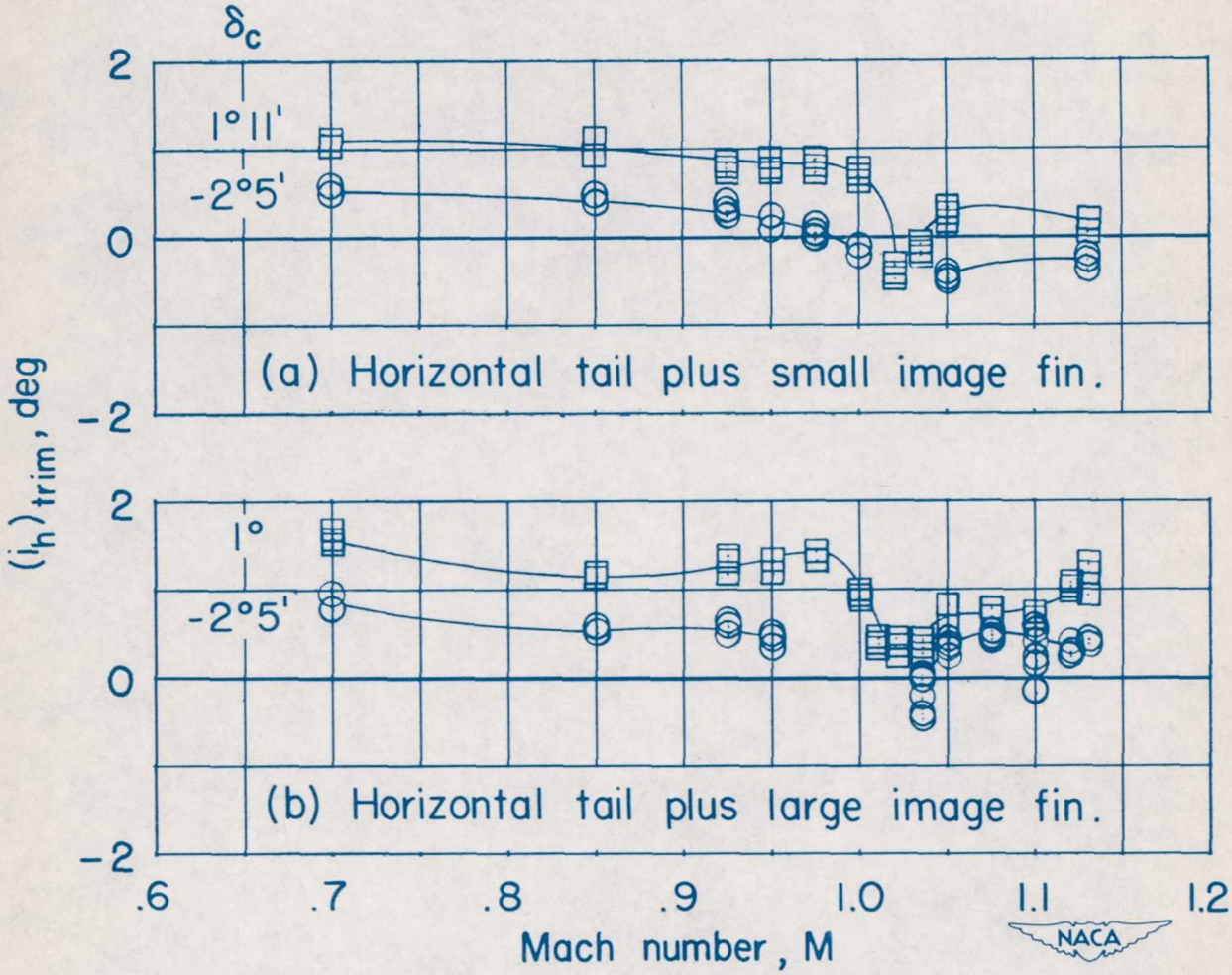

Figure 19.- Variation of floating angle of horizontal tail with image fin against Mach number for 1/7-scale model of complete tail of Grumman XF10F-1 airplane mounted on 3° conical support body. $\alpha_b = 0°$.

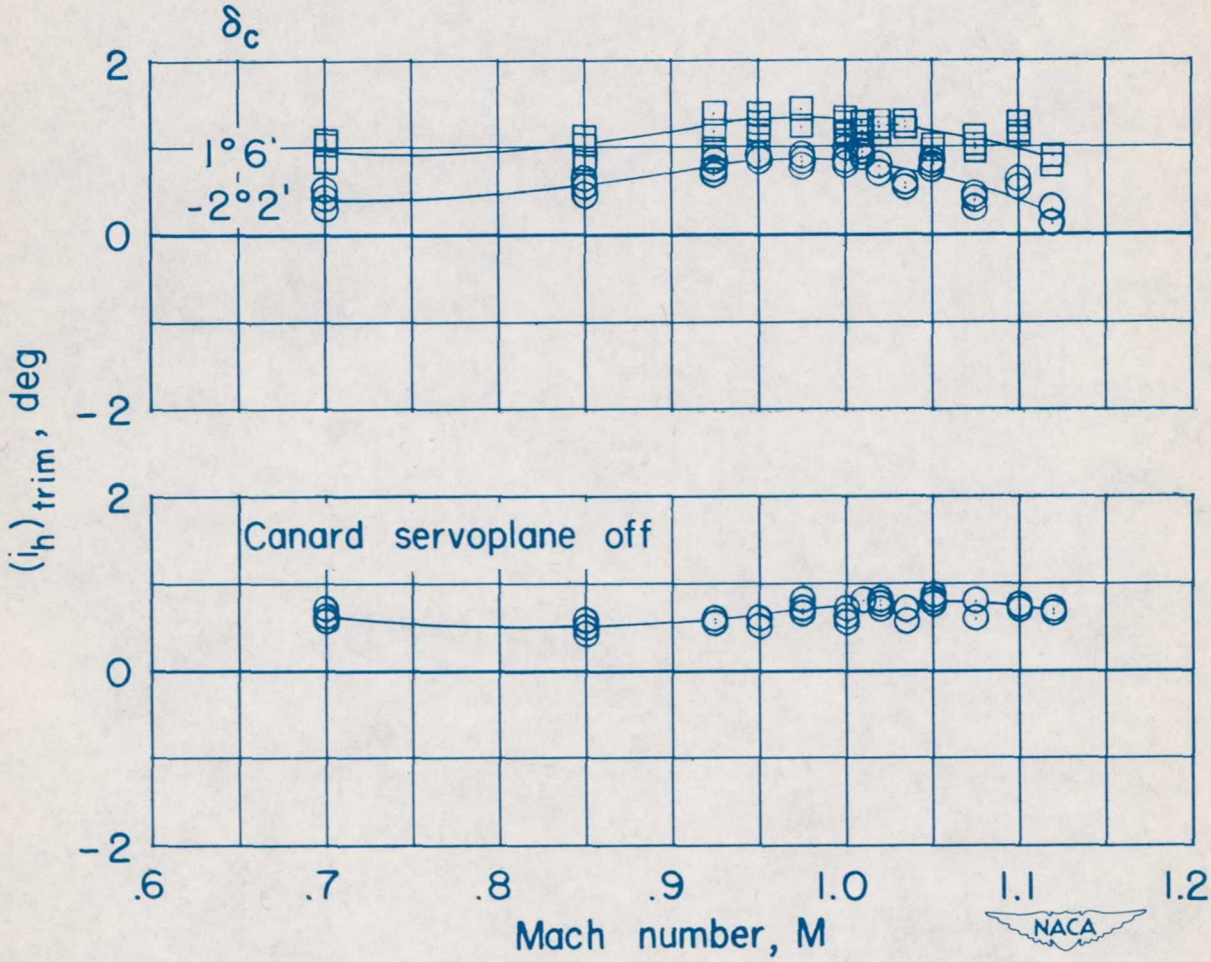

Figure 20.- Variation of floating angle of horizontal tail against Mach number for 1/7-scale model of horizontal tail of Grumman XF10F-1 airplane in combination with auxiliary small-chord sweptforward vertical tail and mounted on 3° conical support body. $\alpha_b = 0^\circ$.

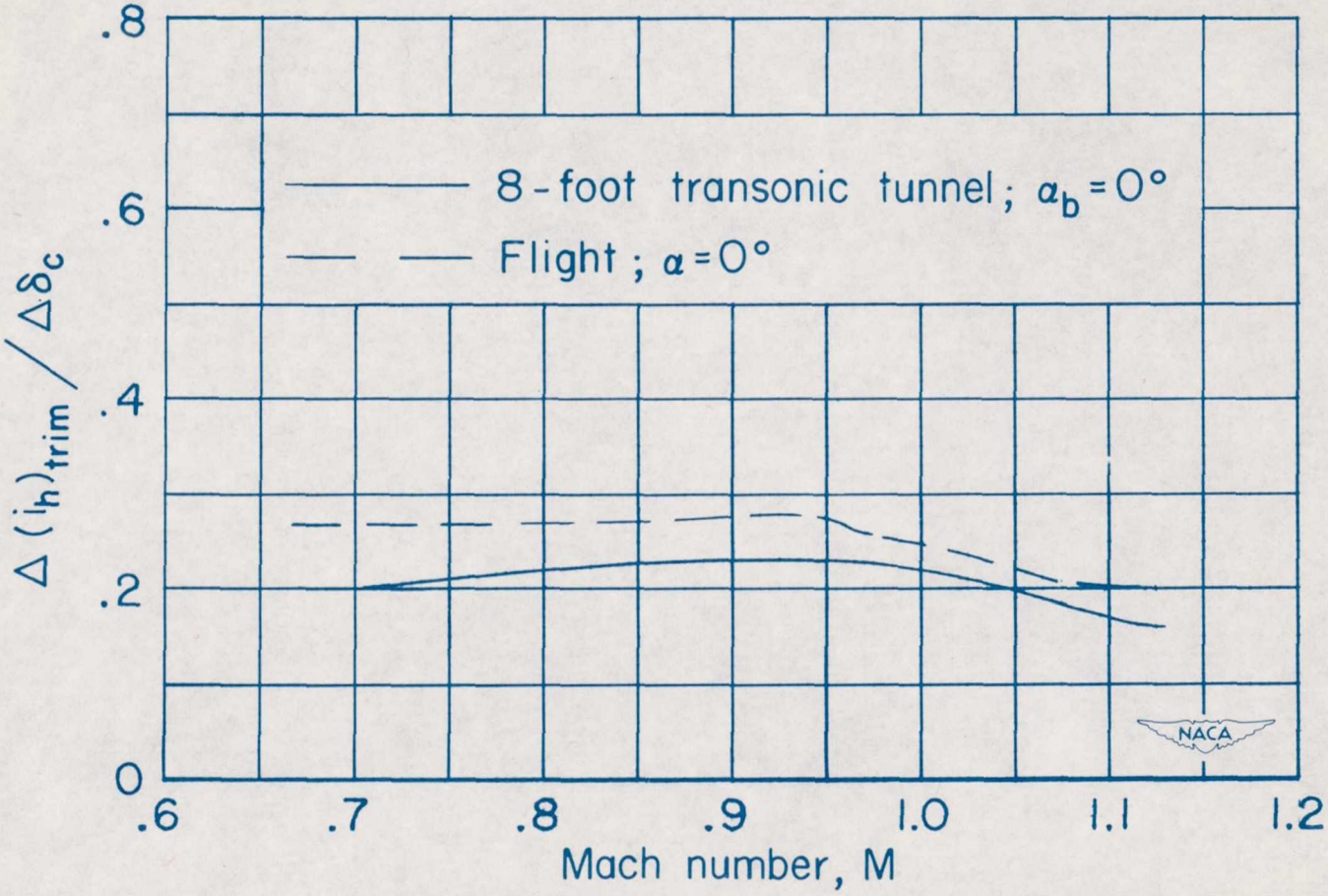

Figure 21.- Canard servoplane effectiveness against Mach number for 1/7-scale model of complete tail of Grumman XF10F-1 airplane.

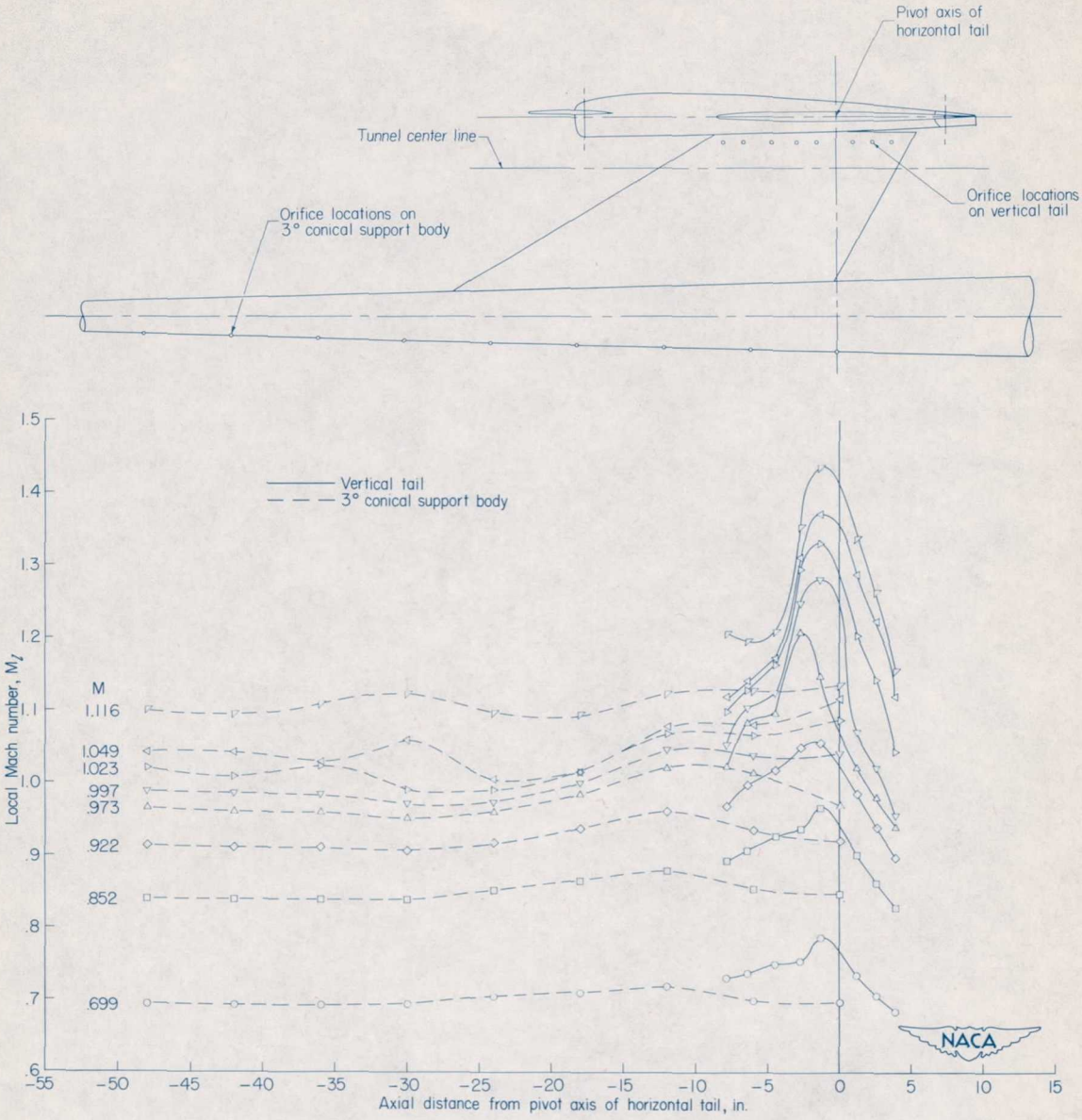

(a) Surface Mach number distributions. $\delta_c = 1^\circ 6'$.

Figure 22.- Surface Mach number distributions and schlieren photographs for 1/7-scale model of complete tail of Grumman XF10F-1 airplane mounted on 3° conical support body. $\alpha_b = 0^\circ$.

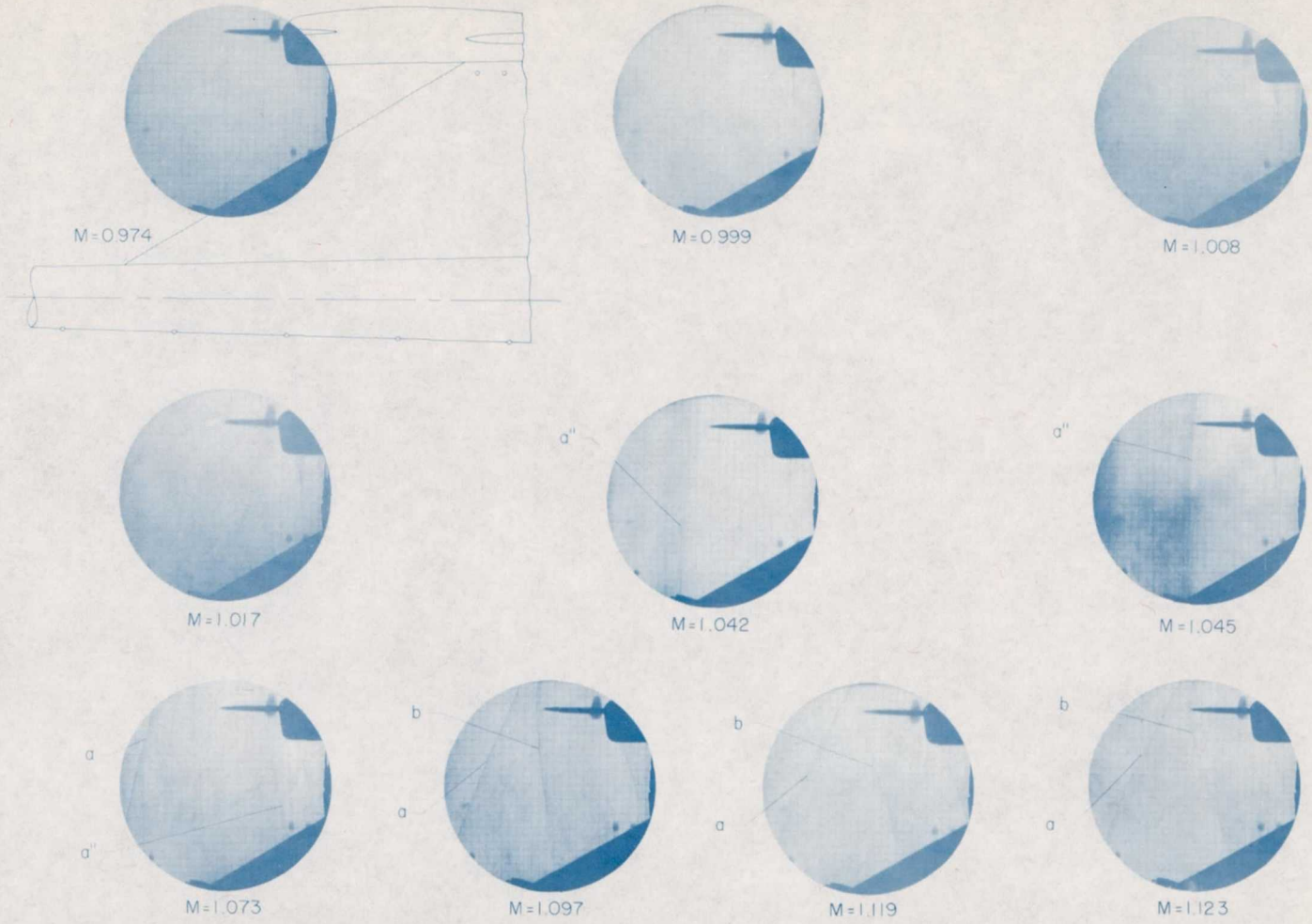

(b) Schlieren photographs at boom nose. $\delta_c = 1^{\circ}12'$.

L-79250

Figure 22.- Continued.

CONFIDENTIAL

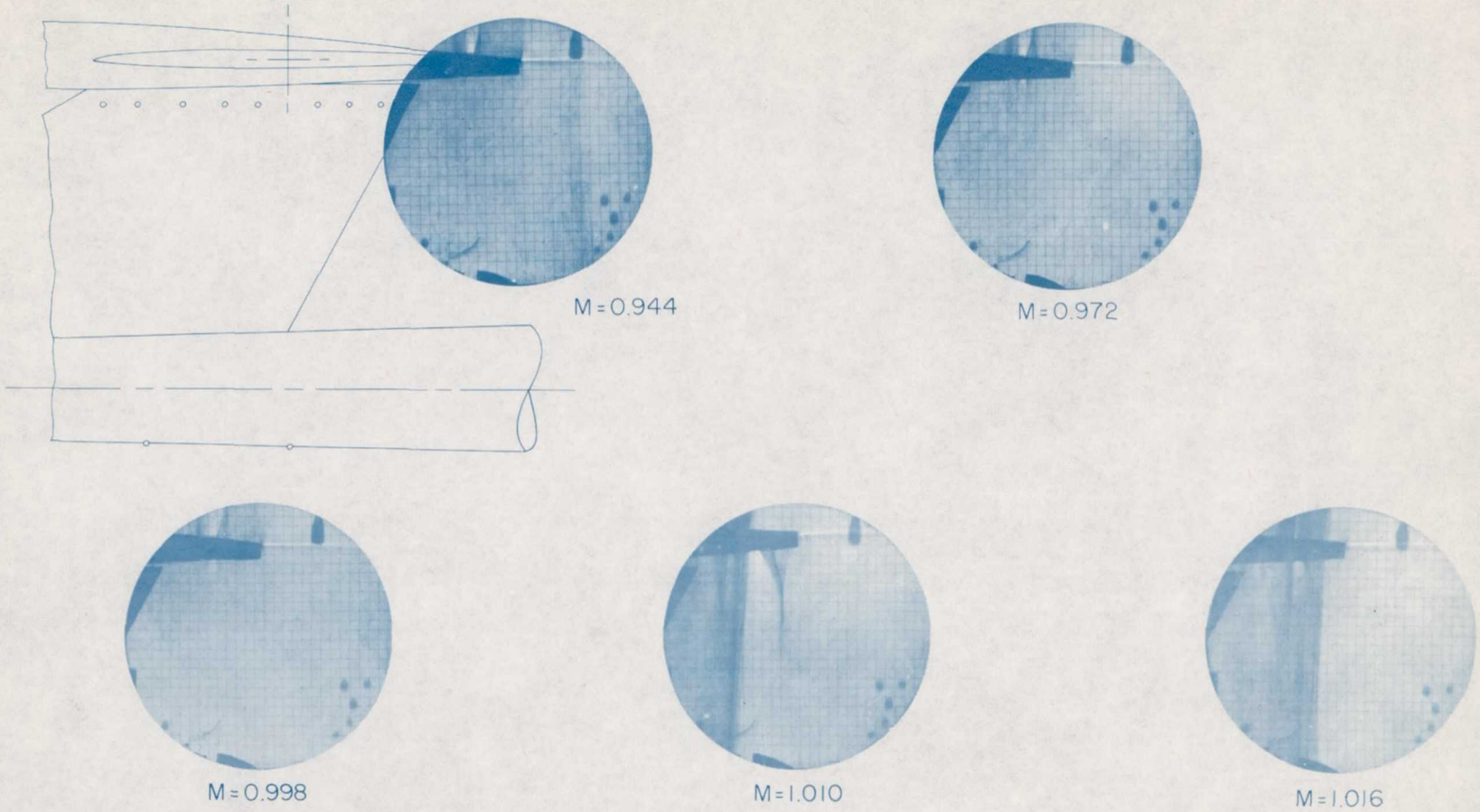

(c) Schlieren photographs at boom base. $\delta_c = 1^{\circ}12'$.

L-79251

Figure 22.- Concluded.

CONFIDENTIAL

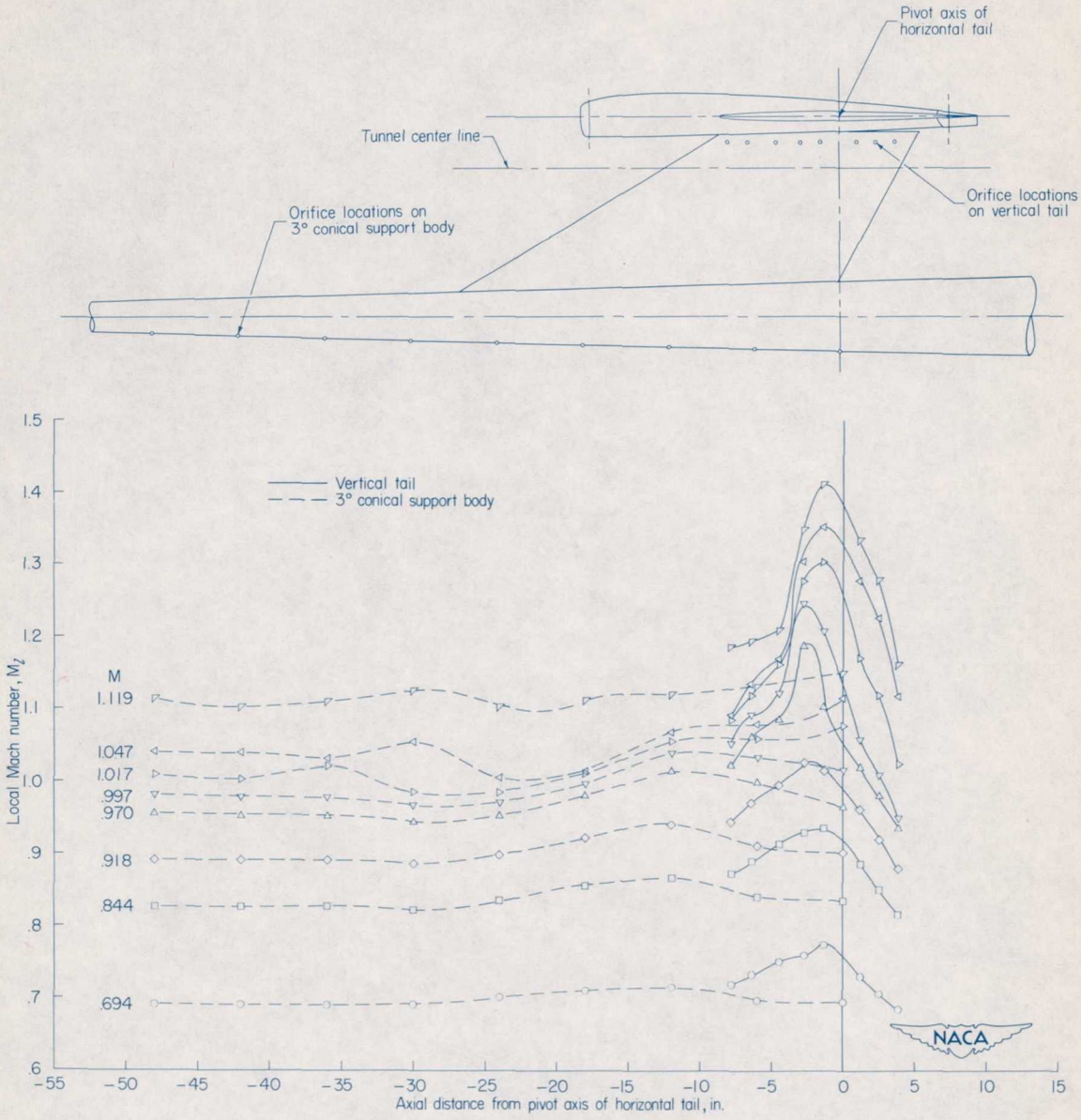

(a) Surface Mach number distributions.

Figure 23.- Surface Mach number distributions and schlieren photographs for 1/7-scale model of complete tail less canard servoplane of Grumman XF10F-1 airplane mounted on 3° conical support body. $\alpha_b = 0^\circ$.

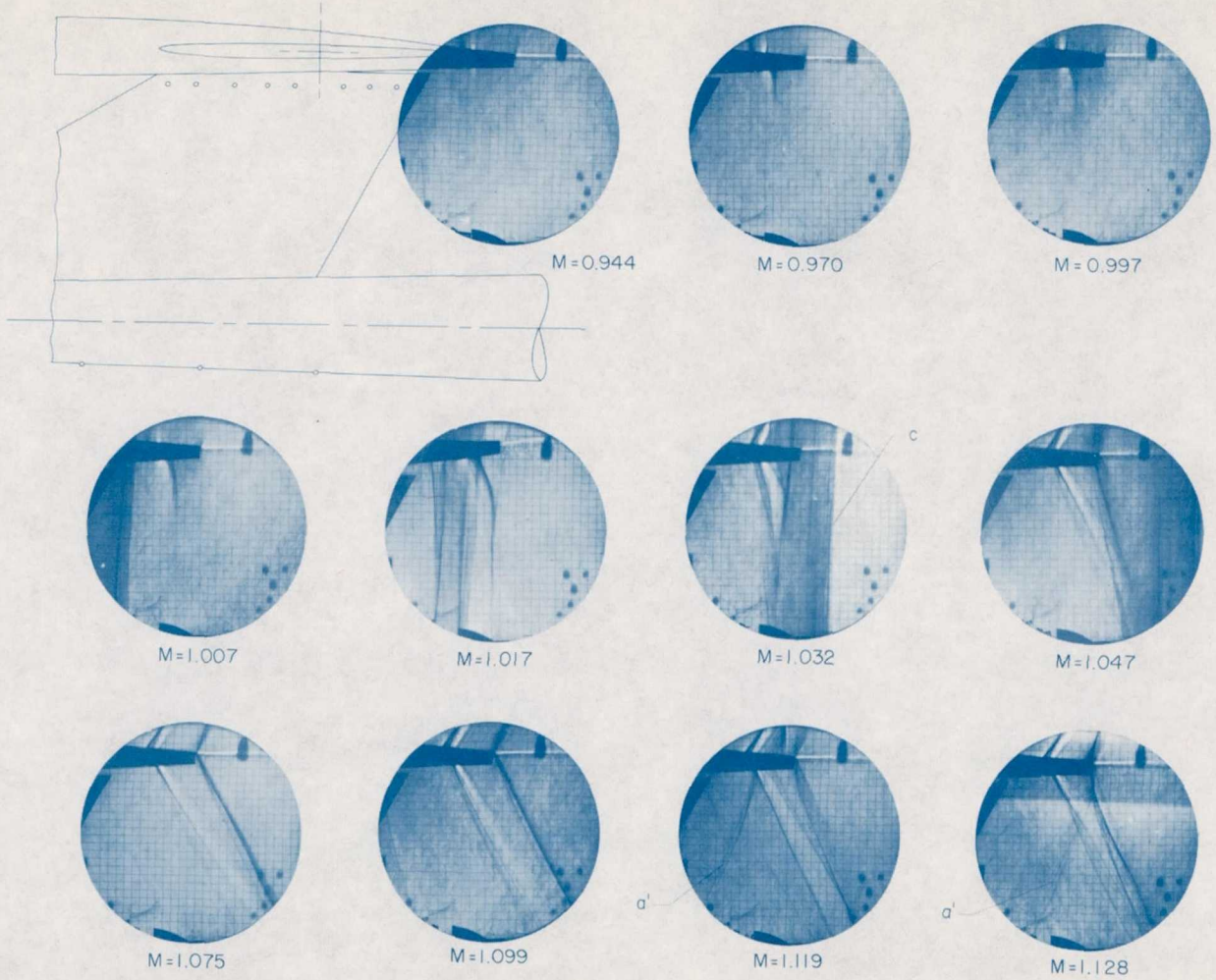

(b) Schlieren photographs at boom base.

Figure 23.- Concluded.

NACA

L-79252

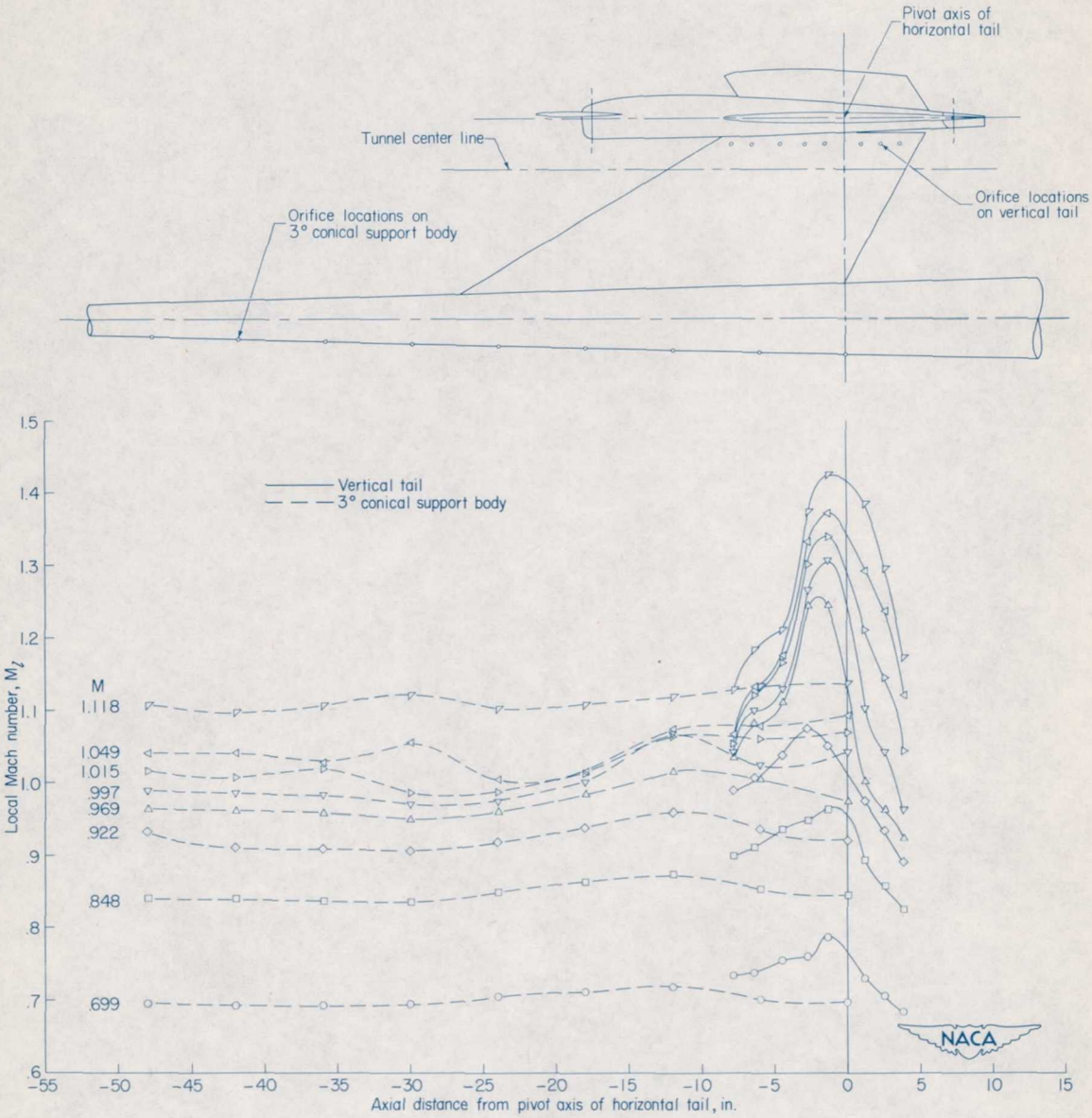

Figure 24.- Surface Mach number distributions for 1/7-scale model of complete tail plus small image fin of Grumman XF10F-1 airplane mounted on 3° conical support body. $\alpha_b = 0^{\circ}$; $\delta_c = 1^{\circ}11'$.

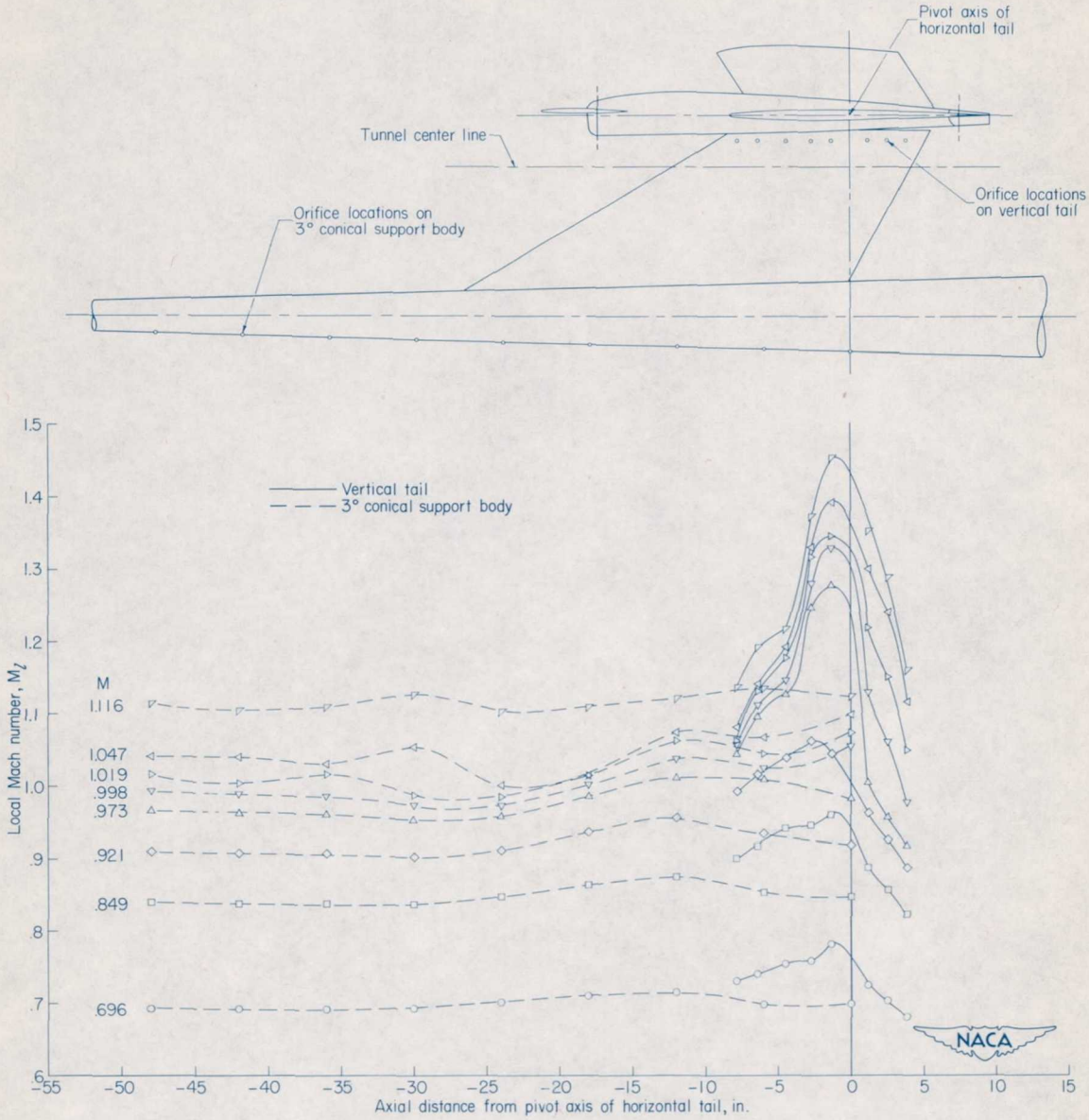

(a) Surface Mach number distributions.

Figure 25.- Surface Mach number distributions and schlieren photographs for 1/7-scale model of complete tail plus large image fin of Grumman XF10F-1 airplane mounted on 3° conical support body. $\alpha_b = 0^\circ$; $\delta c = 1^\circ 0'$.

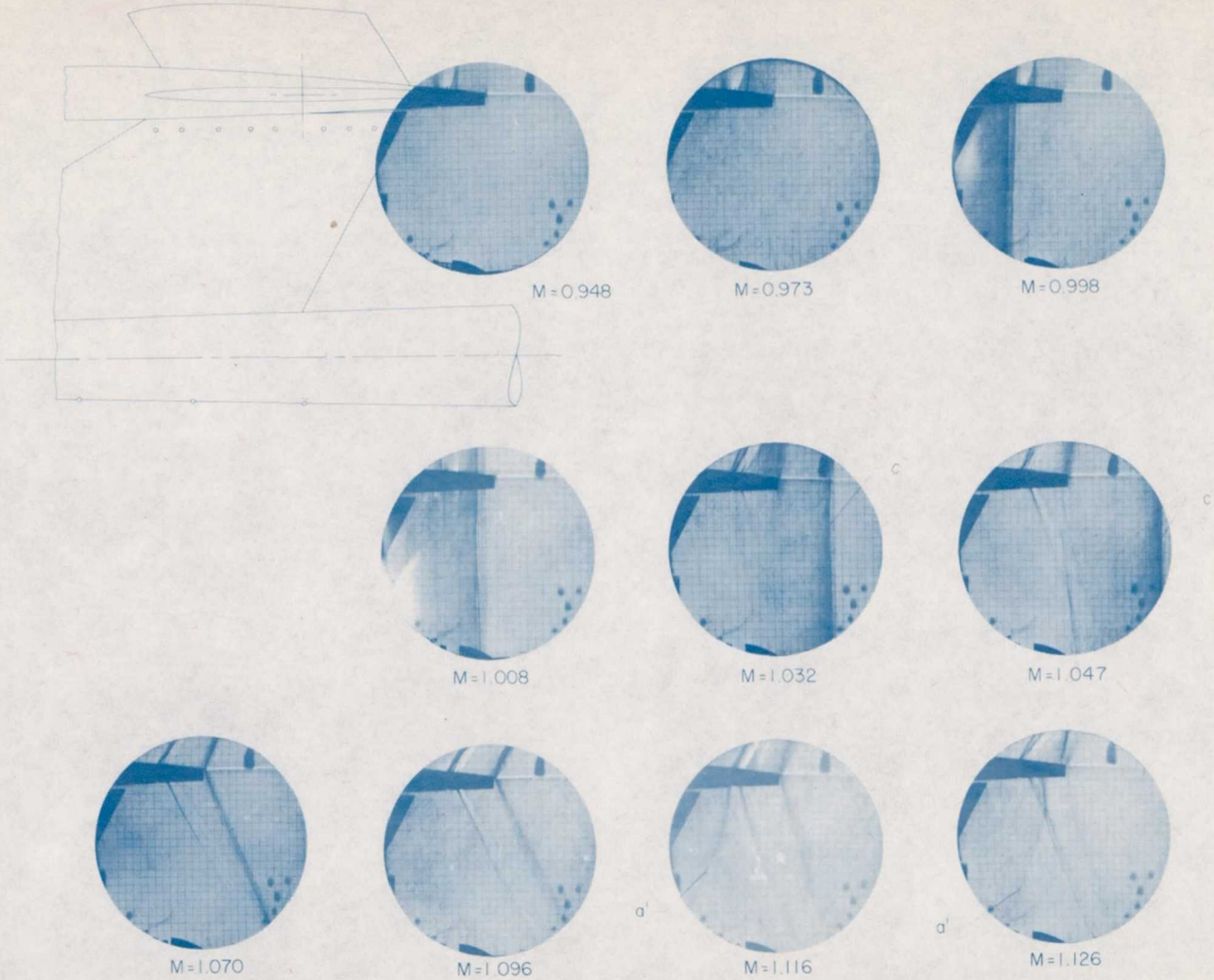

(b) Schlieren photographs at boom base.

Figure 25.- Concluded.

NACA
L-79253

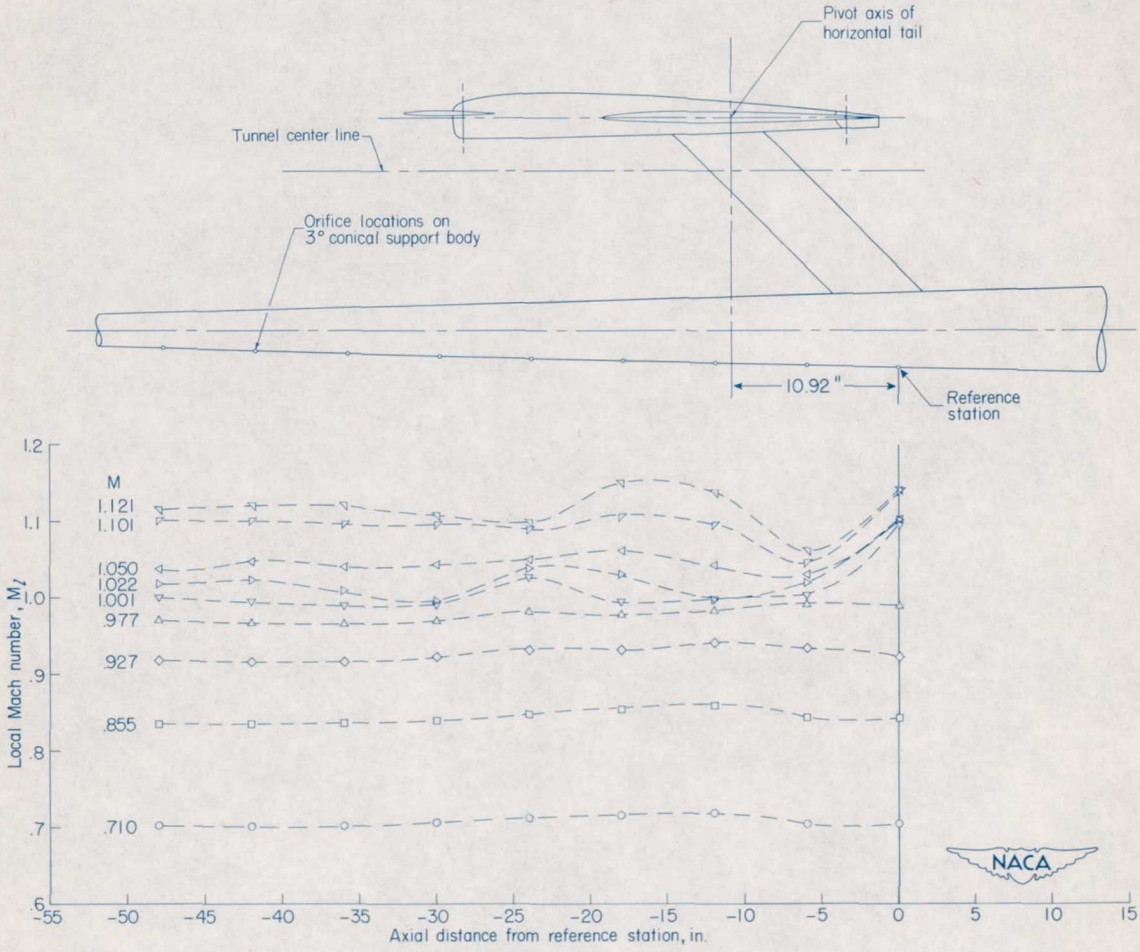

(a) Surface Mach number distributions.

Figure 26.- Surface Mach number distributions along 3° conical support body and schlieren photographs for 1/7-scale model of horizontal tail of Grumman XF10F-1 airplane in combination with auxiliary small-chord sweptforward vertical tail and mounted on 3° conical support body. $\alpha_b = 0^\circ$; $\delta_c = 1^\circ 6'$.

CONFIDENTIAL

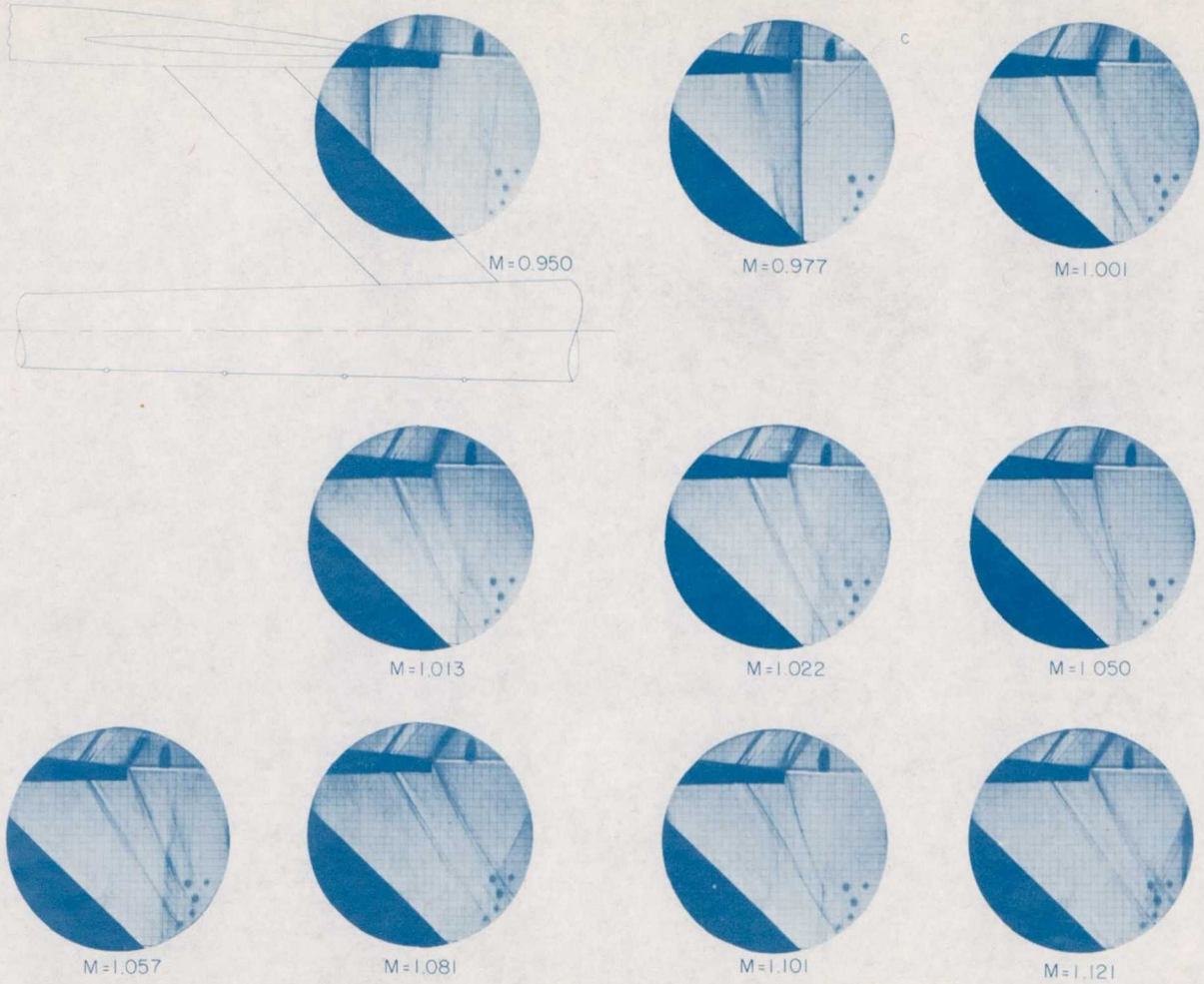

(b) Schlieren photographs at boom base.

Figure 26.- Concluded.

L-79254

CONFIDENTIAL

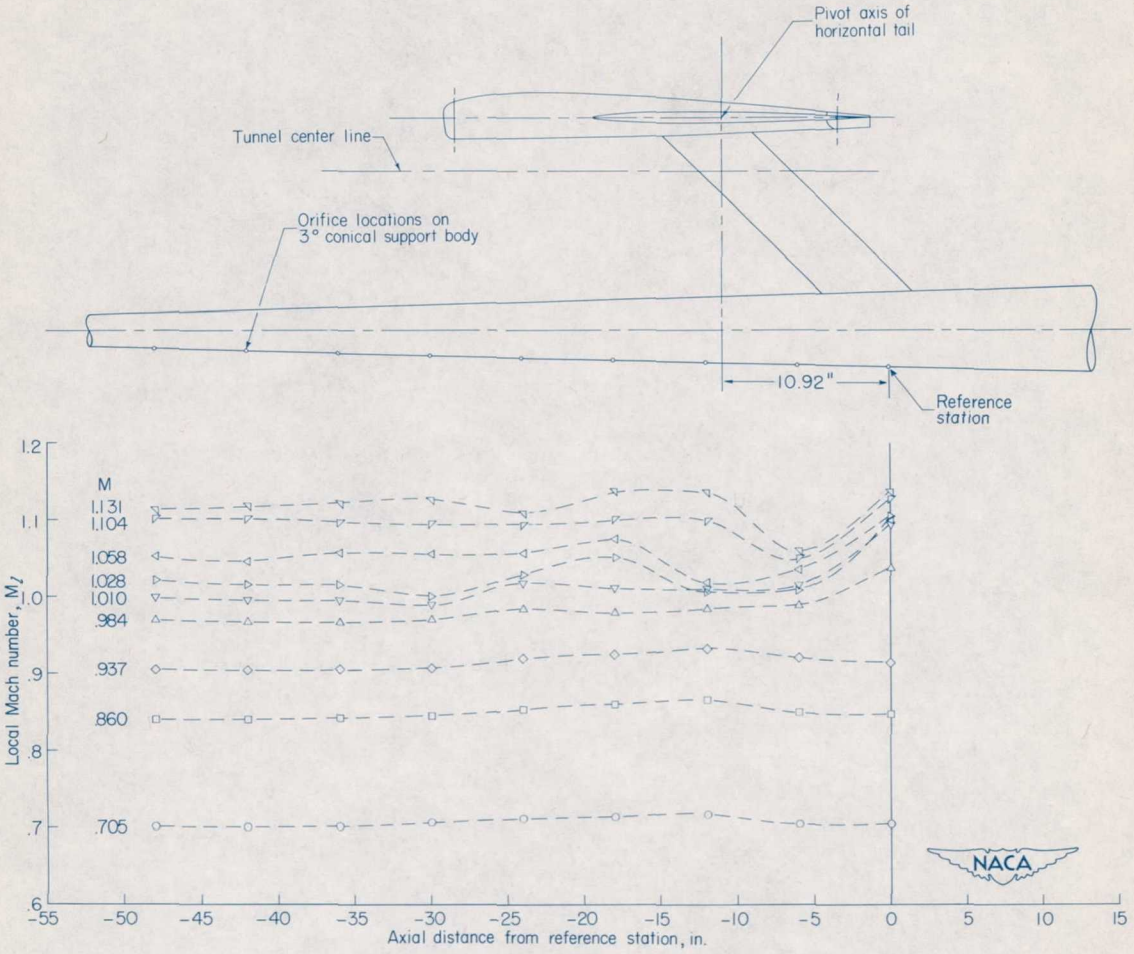

(a) Surface Mach number distributions.

Figure 27.- Surface Mach number distributions along 3° conical support body and schlieren photographs for 1/7-scale model of horizontal tail less canard servoplane of Grumman XF10F-1 airplane in combination with auxiliary small-chord sweptforward vertical tail and mounted on 3° conical support body. $\alpha_b = 0^\circ$.

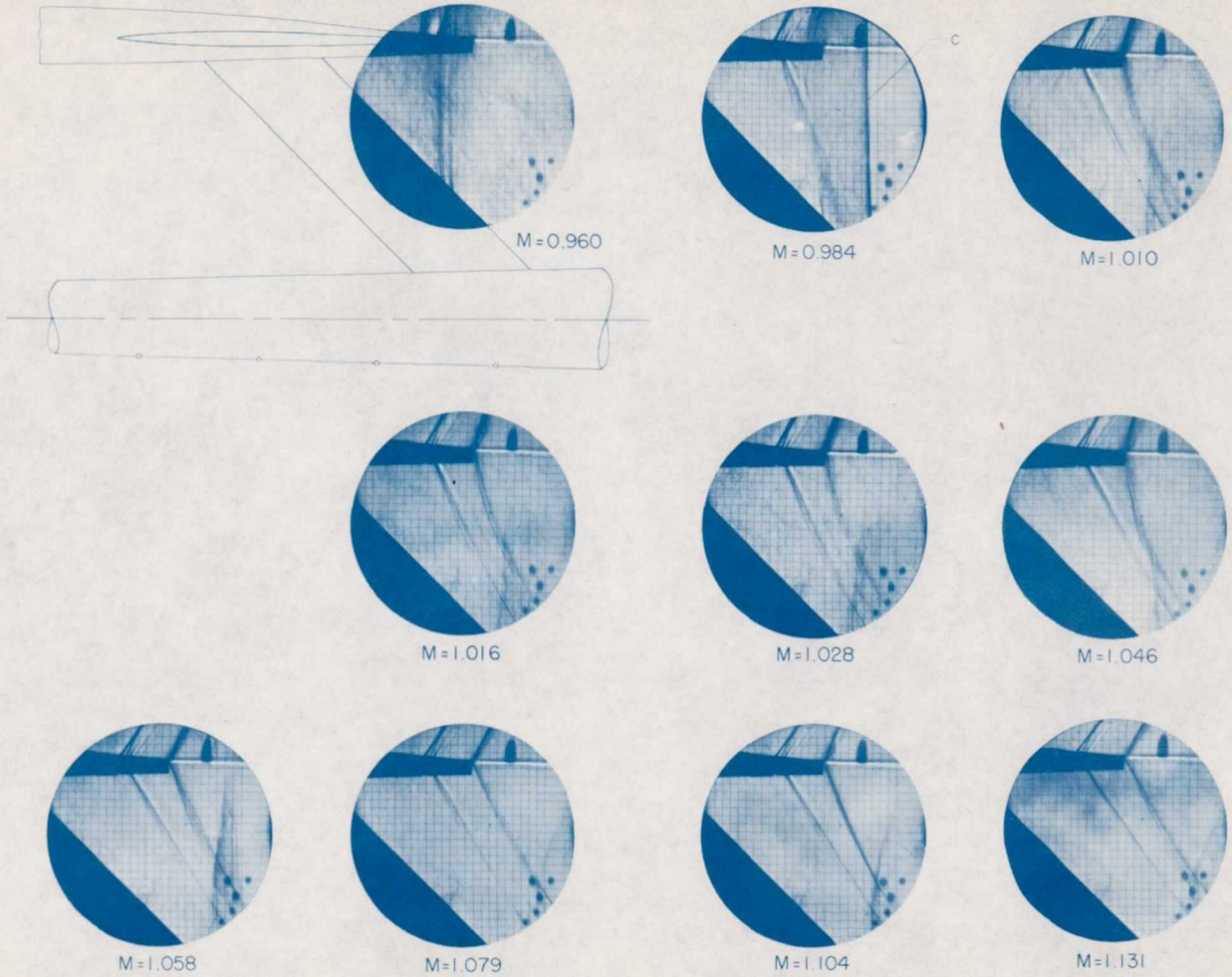

(b) Schlieren photographs at boom base.

Figure 27.- Concluded.

L-79255